A STUDY OF THE INITIATION OF YIELDING IN MILD STEEL

Thesis by
Thad Vreeland, Jr.

In Partial Fulfillment of the Requirements

for the Degree of

Doctor of Philosophy

California Institute of Technology

Pasadena, California

1952

ACKNOWLEDGMENTS

The author wishes to express his sincere appreciation to Professors Donald S. Clark and David S. Wood who directed this research and whose aid and encouragement made this work possible. The assistance of Professors H. Frederic Bohnenblust and George W. Housner who contributed valuable suggestions on the theoretical analysis of this thesis is also acknowledged with thanks.

The rapid-load testing machine was constructed by the California Institute of Technology under a contract with the United States Air Force. Appreciation is expressed to the U. S. Air Force for permission to use the machine. The testing program was conducted under a contract with the Office of Naval Research, United States Navy. Appreciation is expressed to this agency for its sponsorship of the work.

ABSTRACT

This thesis presents the results of an experimental investigation of the behavior of an annealed low-carbon steel subjected to rapidly applied constant stress and to repeated short duration stress-pulses. The magnitude of the stresses in the short duration stress-pulses was greater than the upper yield stress. The material was aged at various temperatures between stress-pulses, and the effect of the time of aging on the number of stress-pulses to induce yielding was determined.

Plastic and anelastic microstrain of 4×10^{-6} in./in. to 37×10^{-6} in./in. is observed prior to the onset of yielding in rapidly applied constant stress tests and in repeated stress-pulse tests. The relation between equilibrium microstrain and stress is determined for stresses below the static upper yield stress. Aging of the specimens for a sufficient length of time at a given temperature between stress-pulses induces recovery in the material such that yielding does not occur in repeated stress-pulse and aging cycles. The activation energy of the recovery process corresponds, within the limits of the experimental accuracy, to the activation energies of carbon and nitrogen diffusion in the material.

These effects are discussed in terms of the dislocation theory of yielding. The recovery process is attributed to the diffusion of carbon and nitrogen to dislocations which have been displaced, thus stabilizing the array of dislocations for the particular stress condition.

Equilibrium microstrain produced by a particular configuration of dislocations is theoretically investigated. An electrostatic analogy of the dislocation model is used in estimating the microstrain. Comparison of the theory and the experimental data leads to the determination of a characteristic length of dislocation which agrees with previous concepts of a mosaic block structure. The delayed yield phenomenon may be qualitatively described by the action of the theoretical dislocation model.

TABLE OF CONTENTS

LIST OF TABLES

LIST OF FIGURES

LIST OF FIGURES (continued)

INTRODUCTION

The dependence of yield point and strain-aging phenomenon on carbon and nitrogen in steel has been studied by other investigators. Muir (1)* and Davenport and Bain (2) have demonstrated that the activation energy of strain aging (return of the yield point) is almost exactly that for the diffusion of carbon in alpha iron. Several other investigators have demonstrated that the presence of the upper yield point in low-carbon steel is intimately related to the presence of carbon and nitrogen (3), (4), (5). The upper yield point and strain-aging phenomenon have been theoretically described by the concept of dislocations and their interaction with interstitial solute atoms, such as carbon and nitrogen in the steel (6), (7), (8), (9).

The theory of Cottrell and Bilby (9) is based upon the ability of interstitially dissolved carbon or nitrogen atoms to inhibit the motion of dislocations. The interstitial atoms relieve hydrostatic tension stress in the dilated portion of the dislocation field which produces an interaction energy between the dislocation and the interstitial atom. Thus, the interstitial atoms tend to diffuse to preferred positions in the dislocation field, forming an atmosphere around the dislocation. A concentration of carbon atoms of the order of 0.001 per cent is sufficient to form saturated atmospheres around all of the dislocations in annealed alpha iron.

A dislocation with a complete or partially formed atmosphere cannot move freely when external stresses are applied to the material. The energy required to release a dislocation from its atmosphere is a

*Figures appearing in parenthesis refer to the references listed at the end of this thesis.

function of the applied stress, and Cottrell and Bilby have made an approximate computation of this function. If a sufficiently high stress is applied, a dislocation may be separated from its atmosphere and move through the material. The separation process may be aided by fluctuations of thermal energy. A thermal activation of the separation process indicates a possible time dependence for the initiation of plastic deformation under constant stress.

Previous investigations in the Impact Laboratory of the California Institute of Technology (10), (11), (12), (13), (14), and (15) have shown that a definite period of time is required for the initiation of yielding in annealed low-carbon steel subjected to a rapidly applied constant stress exceeding the static upper yield stress. The time required for the initiation of yielding has been called the delay time and its dependence on stress and temperature has been determined. Clark and Wood (15) have shown that a single activation energy does not adequately describe the temperature dependence of the delay time. This indicates that the delayed yield cannot be explained by a process involving only the escape of dislocations from their atmospheres of interstitial solute atoms in the manner of the Cottrell-Bilby theory.

The purpose of the present investigation is to study the delayed yield phenomenon in order to gain a more complete understanding of its mechanism. Two experimental techniques are employed:

1. To determine whether or not the cumulative time at stress for a series of stress-pulses is the same as the delay time required for the initiation of yielding in a single rapid-loading test. This can be visualized with the aid of Fig. 1. How is the time t_a related to

$t_b = t_1 + t_2 + t_3 + t_4$? Furthermore, the influence on the delay time of aging at different temperatures for different intervals of time between the stress-pulses is to be determined in this study. By considering the concepts of the dislocation theory, one may suspect that if the material is subjected to a stress greater than the static upper yield stress and that stress is released before yielding can take place, some conditioning action occurs which may have a permanent effect on the delay characteristics of the material.

2. To determine whether or not any plastic or anelastic microstrain occurs during the delay time prior to yielding. The occurrence of microstrain during the delay time would indicate that the release of dislocations from their atmospheres and the initiation of yielding do not occur simultaneously.

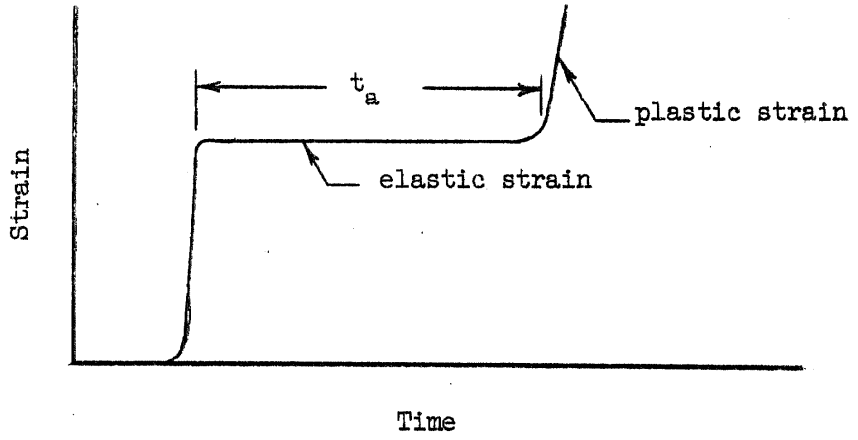

(a) For Rapidly Applied Constant Stress

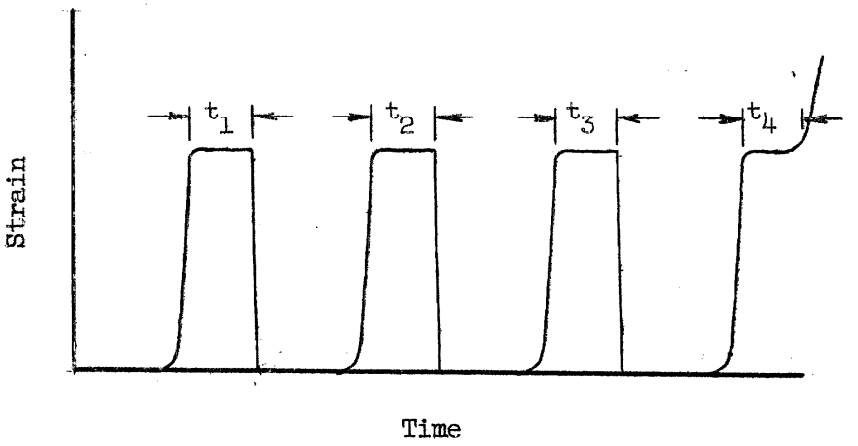

(b) For Stress-Pulses

Fig. 1 Schematic Strain-Time Relations

PREPARATION OF TEST SPECIMENS

Material as Received

The specimens used in this investigation were machined from 5/8 in. diameter, hot-rolled bars from a single billet from heat No. 76889, Columbia Steel Company, Pittsburg, California. Three check analyses made by the mill on random bars all gave the following results:

Carbon	0.12%
Manganese	0.43%
Phosphorus	0.019%
Sulfur	0.042%
Silicon	0.27%
Copper	0.23%
Tin	0.037%

Test Specimen

A drawing of the test specimen used in this investigation is shown in Fig. 2. The gage section was finished by grinding. A thin, flat gage section was employed to facilitate the application of SR-4 strain gages.

Heat-Treatment

Two groups of specimens were employed in this investigation. The first group consisted of specimens which had been annealed for a previous investigation (14), but not tested. These were used for a study of plastic and anelastic microstrain prior to yielding. The original annealing was done in an atmosphere of pure dry hydrogen at a temperature of 1700°F (930°C) for one hour.

The results of a previous investigation (14) indicate that a homogenizing treatment at 1300°F (700°C) for a long period following the annealing treatment brings the material closer to a state of perfect

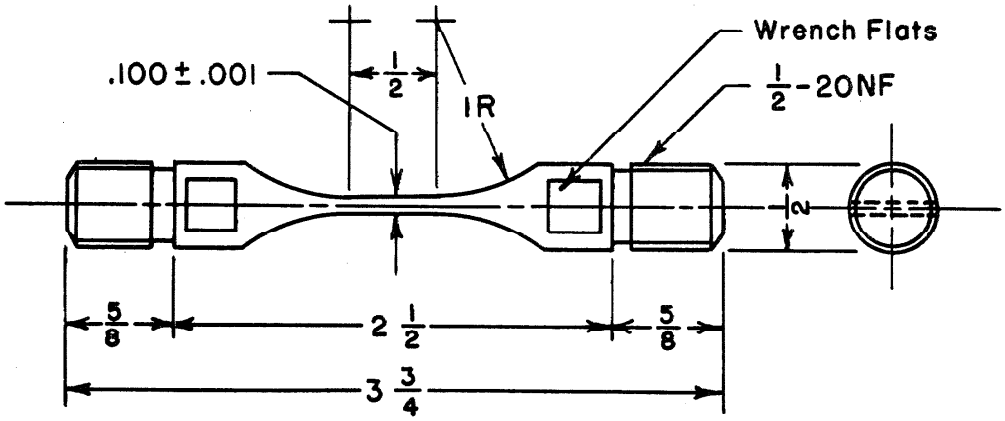

Fig. 2 Test Specimen

equilibrium and considerably reduces the scatter in the rapid-load test data. Such a treatment was given to the second group of specimens, which were used in the present investigation for the static tests, rapid-load tests, and stress-pulse and aging tests. The apparatus used in the heat-treatment is described in reference 14. The hydrogen atmosphere was purified, and a pure hydrocarbon was introduced to prevent specimen decarburization. The hydrogen was treated by passing it through the following equipment prior to entry into the furnace:

(1) De-oxo catalytic hydrogen purifier, a product of Baker and Company, Inc., Newark, New Jersey.

(2) Dri-rite ($CaSO_4$) drying tower.

(3) Normal heptane bath held at 32°F (0°C).

The heat-treatment was as follows:

(1) Annealed at 1680°F (915°C) for 2 1/2 hr.

(2) Homogenized at 1300°F (704°C) for 22 hr.

Photomicrographs of a transverse and longitudinal section of an annealed and homogenized test specimen are shown in Figs. 3 and 4. The A.S.T.M. grain size determined from these photomicrographs is 6.7. The homogenizing treatment did not change the grain size or hardness of the material. The average hardness of the treated material was 54 Rockwell B for 20 determinations with values ranging from 53 to 56. Microscopic examination of the material showed that no detectable change in the amount of pearlite at the surface of the specimen was introduced by the homogenizing treatment. The fact that the hardness of the material was not changed by this treatment also indicates that the carbon content was not changed appreciably.

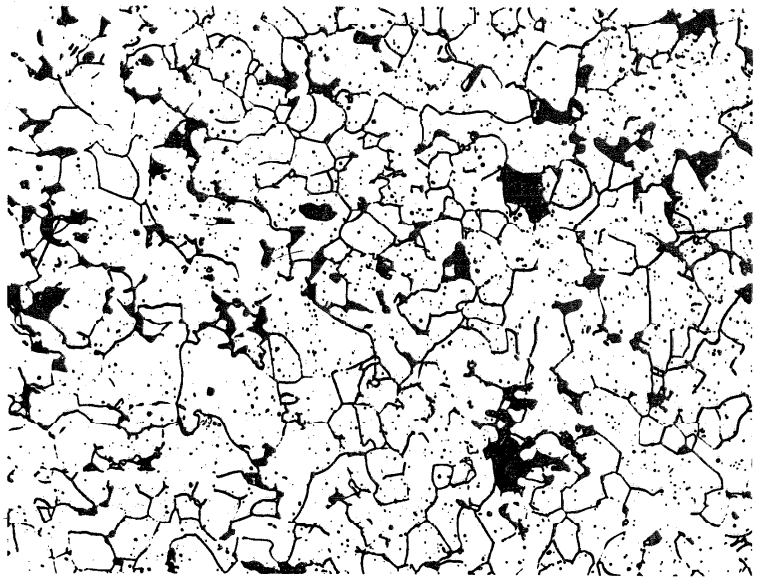

Fig. 3 Microstructure of Transverse Section of Annealed and Homogenized Specimen. Etch 1% Nital. X150

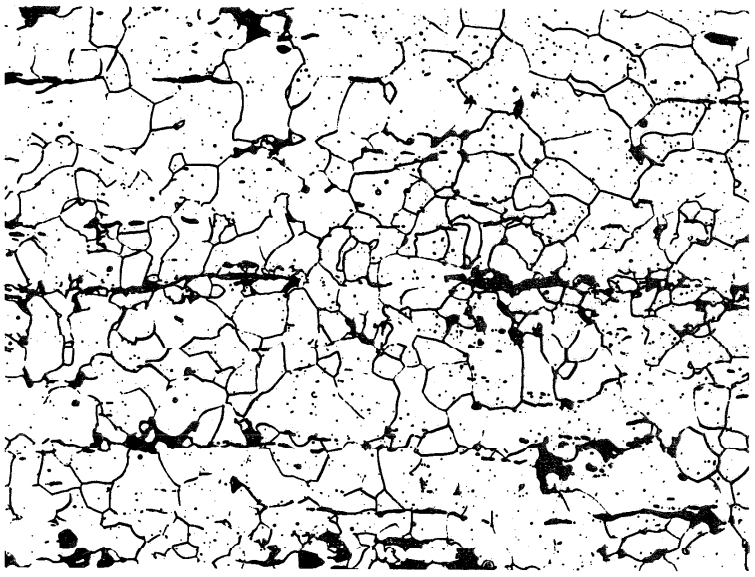

Fig. 4 Microstructure of Longitudinal Section of Annealed and Homogenized Specimen. Etch 1% Nital X150

EQUIPMENT

The tests were made with the rapid-load testing machine described in reference 10. Suitable alteration of a part of the actuating mechanism permits the application of a stress-pulse to the test specimen. The actuating cam used in previous tests and the new cam by which the stress-pulse can be obtained are shown in Fig. 5. The stress is applied to the specimen when the follower moves down the cam surface; the stress remains constant until the follower is forced up by the second sloping cam surface which unloads the specimen. The duration of the stress-pulse may be varied from approximately 20 to 150 millisec by varying the cam speed.

The extensometers described in reference 13 were used for tests in which only the initiation of yield strain was to be detected. Tensile and bending strains were measured by means of SR-4 resistance-sensitive wire strain gages. One type A-5 gage was bonded to each side of the gage section of the test specimen. Suitable electrical connections between the specimen gages and temperature-compensating dummy specimen gages completed the strain gage bridge circuits.

Plastic and anelastic microstrain was measured by employing a strain bar which was attached to one end of the specimen. The nominal dimensions of the gage section of the specimen and the strain bar are the same; hence, the elastic strains in the specimen and the bar are nearly equal. The strain bar is made of X4130 steel, heat-treated so that it remains elastic under the loads used in this investigation. Two type A-5 gages are bonded to the gage section of the strain bar and electrically connected to the two gages bonded to the gage section of the specimen

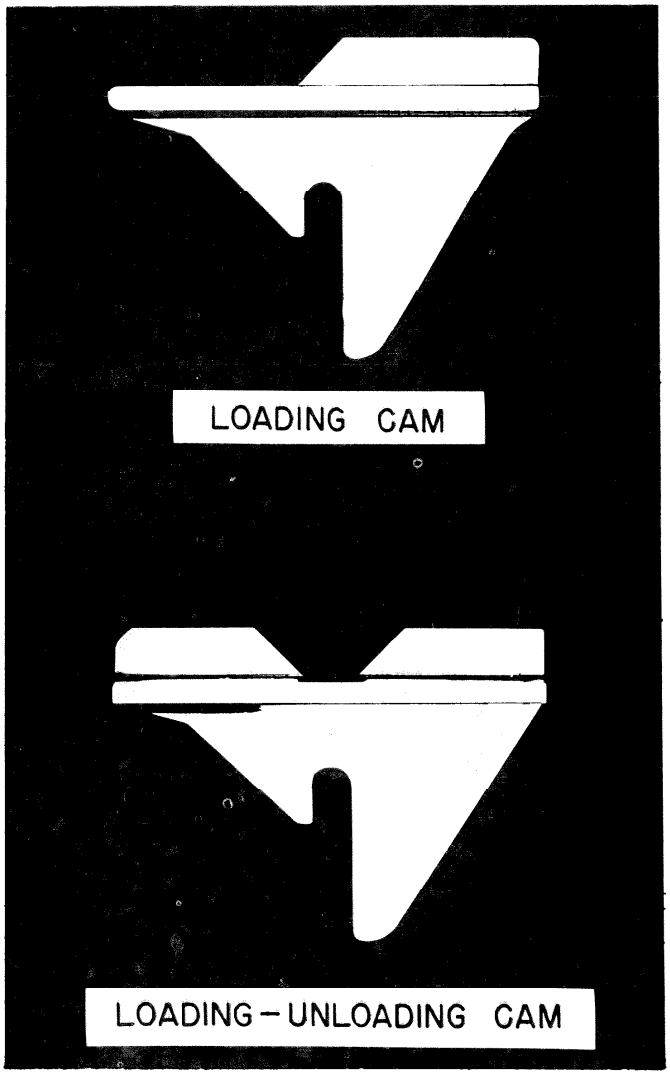

Fig. 5 Loading and Loading-Unloading Cams

in such a manner that the elastic strain in the strain bar is subtracted from the total strain in the specimen. This arrangement permits the use of the maximum possible sensitivity of the recording system without exceeding the total strain-recording capacity of the system.

The load acting on the specimen was measured by means of a dynamometer employing type AB-14, SR-4 strain gages with suitable temperature compensation. The dynamometer was calibrated with an Olsen beam-type universal testing machine. A recent calibration of the testing machine showed the error to be within 0.3 per cent of the indicated load. The dynamometer, specimen, and strain bar are shown in Fig. 6. The cover for the gage section of the strain bar is removed to show the arrangement of the gages.

The signals from the strain gage bridge circuits were recorded on photographic paper by a recording oscillograph manufactured by the Consolidated Engineering Corporation, Pasadena, California. A 3,000 cycle/sec carrier bridge amplification system was used. The natural frequency of the galvanometer elements employed in the oscillograph is 500 cycles/sec. Timing lines at intervals of 0.1 or 0.01 sec are projected onto the test record to provide a time base.

The equipment for aging the specimens at temperatures above room temperature consisted of an oil bath heated by an immersion heater. The temperature was controlled to ±1°F by a Fenwal thermal switch in series with the heater. A stirring motor provided agitation to assure uniform temperature of the bath and to increase the rate of heat transfer to the specimen.

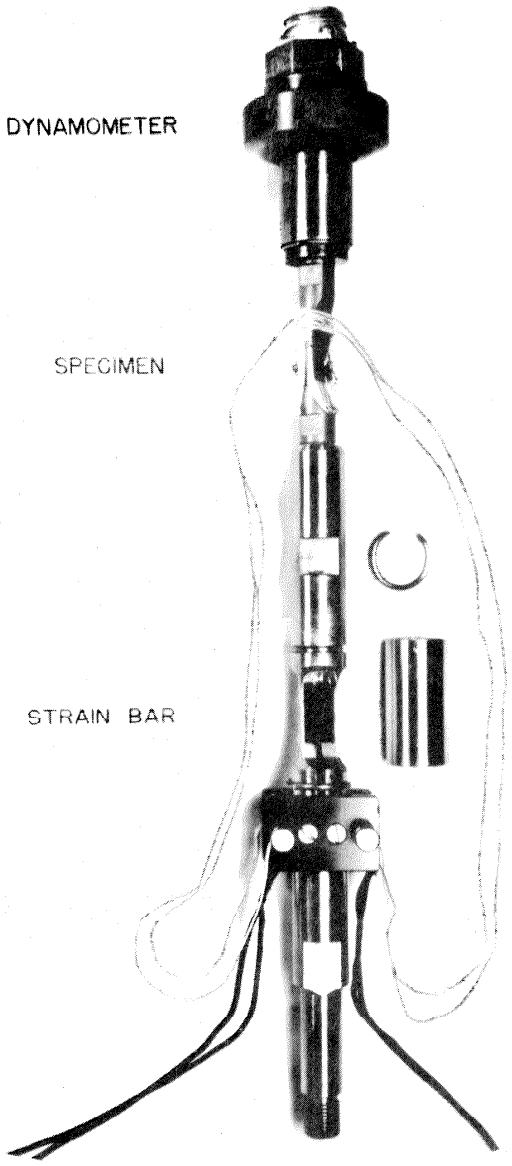

Fig. 6 Dynamometer, Specimen, and Strain Bar

TEST PROCEDURE AND EXPERIMENTAL RESULTS

Static Tension Tests

The static tension tests were performed in the rapid-load testing machine by manual operation of the pressure system. The load was applied to the specimen in increments, and each increment was held for 3 min before recording values of load and tensile strain. When the specimen yielded, the load was removed and then reapplied in increments to determine the lower yield stress. The test was discontinued when the bonded strain gages came loose from the specimen at a strain of aproximately 2 per cent. The static properties of the material are listed in Table I, and static stress-strain curves are presented in Figs. 7 and 16.

Rapid-Load Tension Tests

The rapid-load tension tests which were made to determine the stress-delay time characteristics of the material were performed in the manner described in reference 10. The test results are listed in Table II and plotted in Fig. 8.

The extent of bending in the specimen during rapid-load tension tests was investigated. The maximum bending strain found in nine tests was 6.2 per cent of the tensile strain, and the mean was 2.9 per cent.

Repeated Stress-Pulse Tests

The tests which were employed to study the effect of stress-pulses and aging on the delay time were made by imposing a stress-pulse of essentially constant magnitude and duration on the specimen. The pulse was as follows:

Table I

STATIC PROPERTIES OF THE MATERIAL TESTED

Annealed Material
(Data from Ref. 14)

ASTM Grain Size	Hardness Rockwell B	Specimen Number	Upper Yield Stress 10^3 lb/in.^{2}	Lower Yield Stress 10^3 lb/in.^{2}	Yield Strain %
6.7	54	191	43.8	31.8	1.1
		215	42.5	30.5	1.5

Annealed and Homogenized Material

ASTM Grain Size	Hardness Rockwell B	Specimen Number	Upper Yield Stress 10^3 lb/in.^{2}	Lower Yield Stress 10^3 lb/in.^{2}	Yield Strain %
6.7	54	134	42.5	30.0	> 1.6
		181	41.3	28.0	1.7

Annealed and Homogenized Material
After Stress-Pulse and Aging Treatment

Spec. No.	Stress-Pulse Magnitude 10^3 lb/in.^{2}	Stress-Pulse Duration sec	No. Stress-Pulses	Aging Between Stress-Pulses Temp. °F	Aging Between Stress-Pulses Time min	Upper Yield Stress 10^3 lb/in.^{2}	Lower Yield Stress 10^3 lb/in.^{2}	Yield Strain %
107	45	0.029	14	150	103	43.5	29.5	1.34
122	45	0.029	12	150	103	41.7	28.5	1.4

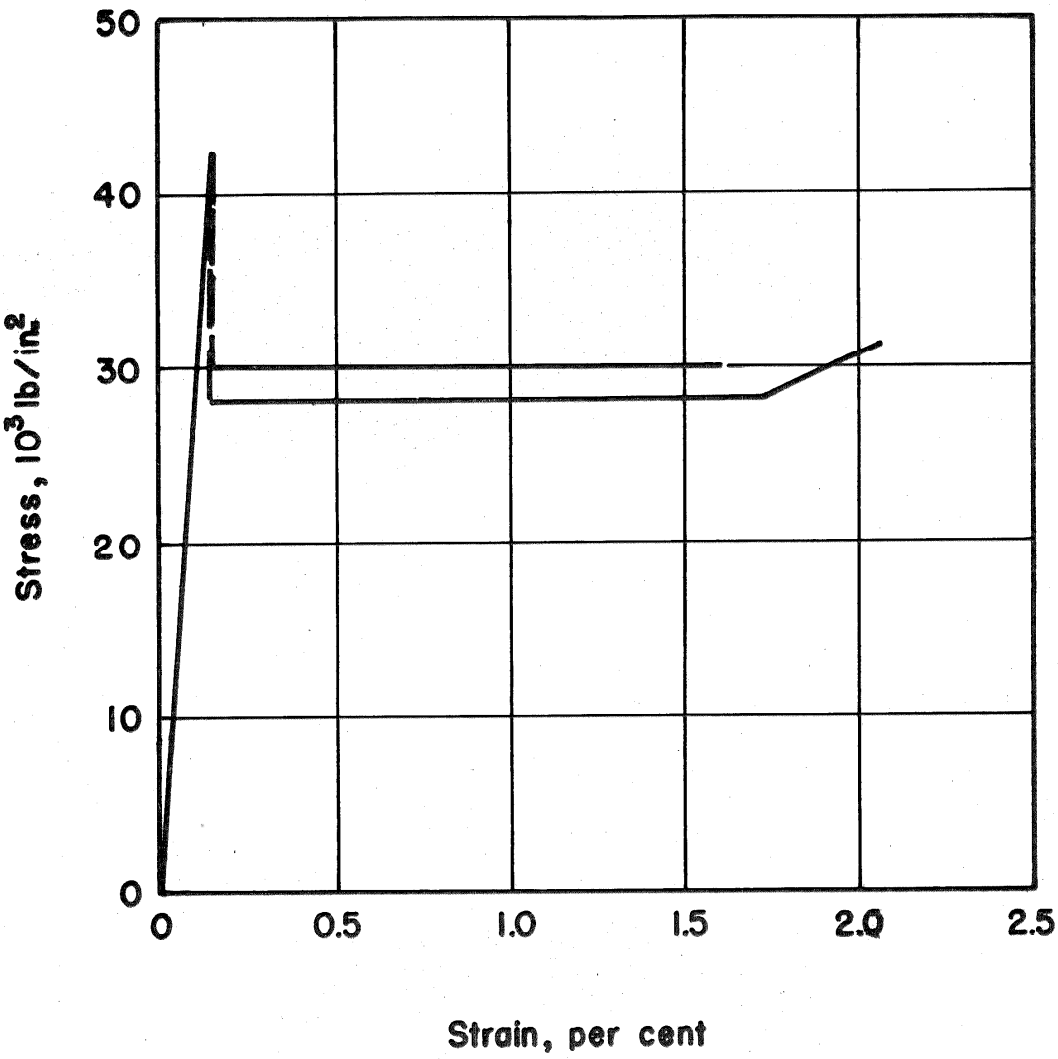

Fig. 7 Static Stress vs. Strain
Annealed and Homogenized Material

Table II

RESULTS OF THE RAPID-LOAD TENSILE TESTS
STRESS-DELAY TIME RELATIONSHIPS

Annealed and Homogenized Material

Specimen Number	Stress 10^3 lb/in.^{2}	Delay Time sec
11	50.0	0.006
10	49.1	0.004
17	47.5	0.008
9	47.2	0.006
26	46.7	0.035
22	46.4	0.047
24	46.2	0.049
27	46.2	0.042
25	46.0	0.022
82	46.0	0.023
21	45.8	0.030
23	45.8	0.038
56	45.8	0.019
33	45.4	0.024
12	44.7	0.093
1	43.4	0.11
2	41.0	0.58
4	38.4	1.79
5	38.4	1.22
6	37.6	0.60
7	35.9	95.1

Annealed and Homogenized Material
After Stress-Pulse and Aging Cycles

Stress-Pulse: Magnitude = 45,000 ±800 lb/in.^{2}
Duration = 0.029 ±0.001 sec

Specimen Number	Cumulative Time of Stress-Pulses sec	Aging Between Stress-Pulses Temp. °F	Aging Between Stress-Pulses Time min	Stress 10^3 lb/in.^{2}	Delay Time sec
105	0.409	150	100	52.5	0.021
58	0.573	200	11	50.7	0.009
72	0.595	200	13	45.1	0.157
73	0.427	200	13	45.0	0.112
41	0.522	200	15	44.5	0.28
40	0.464	200	15	40.7	15.2

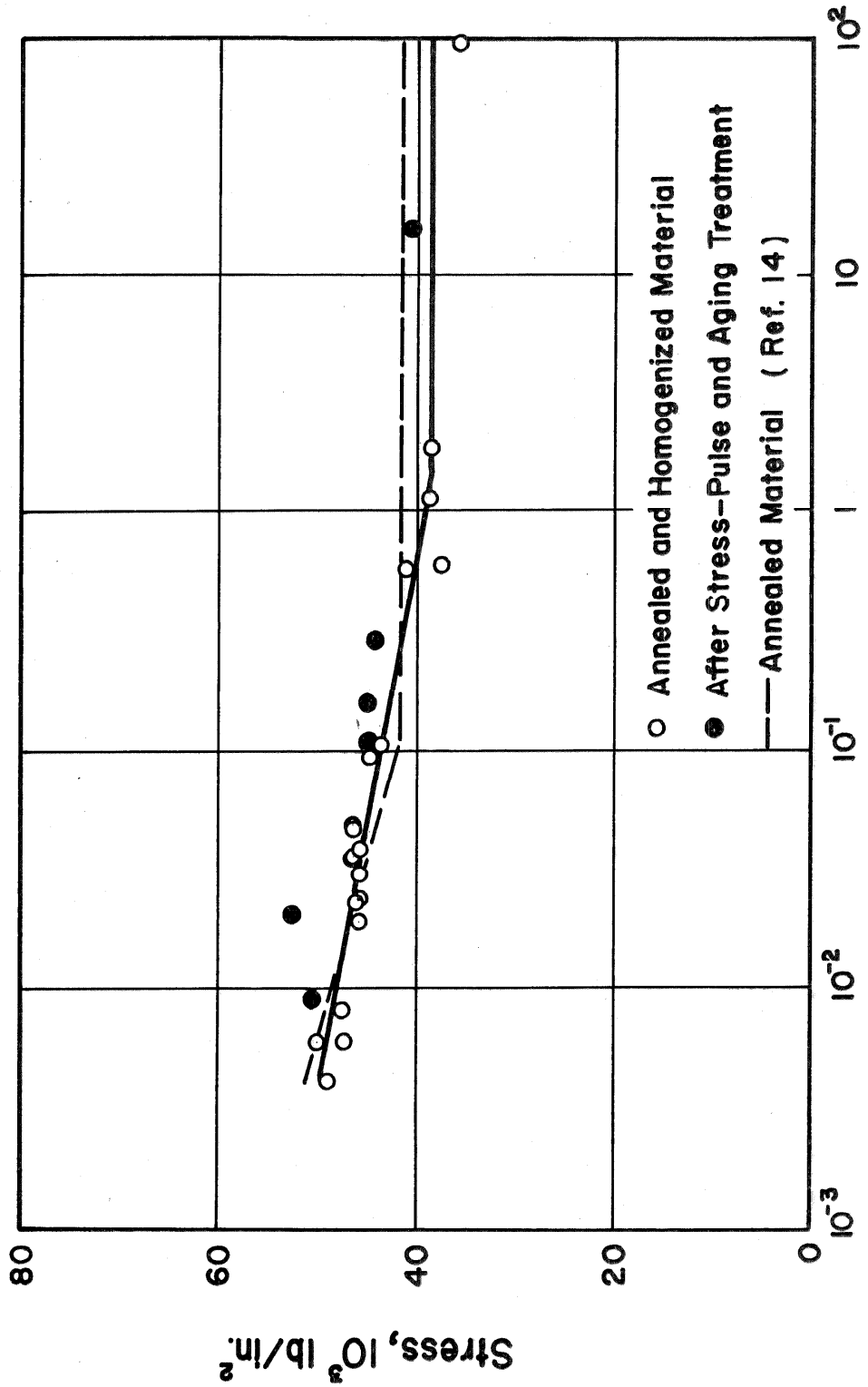

Fig. 8. Delay Time vs. Stress

(1) Stress of 45,000 ±800 lb/in.^{2} applied in approximately 0.007 sec.

(2) Stress held essentially constant for 0.029 ±0.001 sec.

(3) Stress removed in approximately 0.003 sec.

The delay time for the material when subjected to a stress of 45,000 lb/in.^{2} is approximately 0.050 sec which is greater than the duration of one stress-pulse and less than the duration of two stress-pulses. Thus, the material might be expected to yield during the second stress-pulse if there is no recovery between pulses. This procedure provides a method of detecting any recovery that may occur between stress-pulses.

The specimens were aged for various intervals of time between stress-pulses at temperatures of 70°F (21°C), 150°F (66°C), and 200°F (93°C). The procedure of aging the specimen at 150°F and 200°F after a stress-pulse was as follows:

(1) Specimen removed from rapid-load machine and placed in oil bath at desired temperature within five minutes after stress-pulse.

(2) Specimen removed from oil bath after desired aging period and immediately cooled in powdered dry ice (-109°F or -78°C).

(3) Specimen brought to approximately 70°F in an alcohol bath five minutes prior to next stress-pulse.

(4) Stress-pulse applied when specimen reached 70°F; specimen temperature determined by thermocouple and Leeds and Northrup recording potentiometer.

The initiation of yielding was determined with the extensometers in the majority of the stress-pulse tests. Plastic and anelastic microstrain was measured by means of the strain bar in two tests. A typical record of a stress-pulse is shown in Fig. 9.

The results of this series of tests are listed in Table III. The cumulative time at stress before yielding is plotted in Fig. 10 as a function of aging time between stress-pulses for the three aging temperatures. The specimens which were aged at 70°F for 3 min yielded during the second stress-pulse, and the cumulative time at stress before yielding was approximately equal to the normal delay time at the same stress. Aging at 150°F and 200°F for periods equal to or greater than a certain critical value induced recovery from the effects of the previous stress-pulse. This is shown by the fact that yielding did not take place in successive stress-pulse and aging cycles. The data show that recovery is accomplished by aging for a minimum of approximately 12 min at a temperature of 200°F and 100 min at 150°F.

Measurement of Plastic and Anelastic Microstrain

Typical records of microstrain in rapid-load and stress-pulse tests are shown in Figs. 11, 12, and 13. A correction must be applied to the data obtained from these records in order to obtain values of microstrain. This correction is made necessary by an imperfect balance between the elastic strain in the specimen and the strain bar. The sources of the inequality of elastic strain are:

(1) A difference in cross-sectional areas of the strain bar and the specimen.

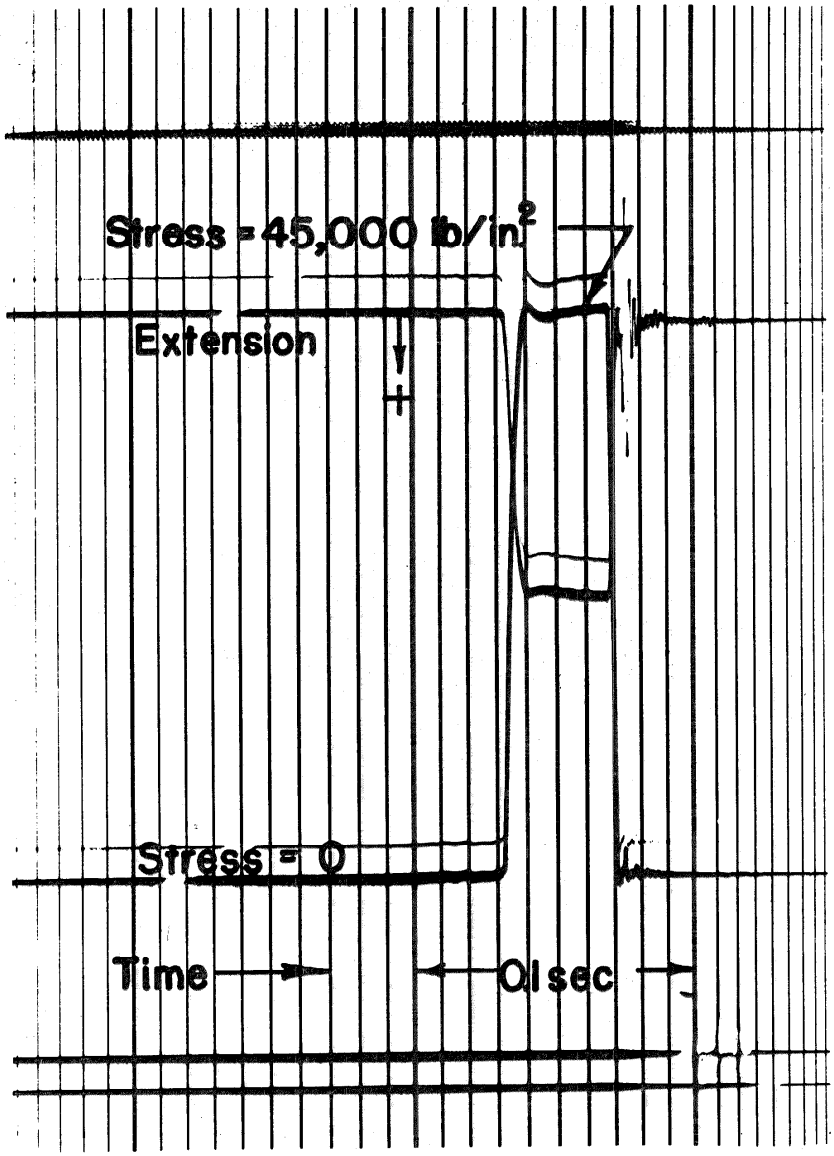

Fig. 9 Typical Record of a Stress-Pulse

Table III

RESULTS OF THE REPEATED STRESS-PULSE TESTS

Annealed and Homogenized Material

Stress-Pulse: Magnitude = 45,000 ±300 lb/in.^{2}
Duration = 0.029 ±0.001 sec

Aging Temperature 70°F Test Temperature 70°F			Aging Temperature 150°F Test Temperature 70°F			Aging Temperature 200°F Test Temperature 70°F		
Spec. No.	Aging Time Between Pulses min	Cumulative Time at Stress Before Yield sec	Spec. No.	Aging Time Between Pulses min	Cumulative Time at Stress Before Yield sec	Spec. No.	Aging Time Between Pulses min	Cumulative Time at Stress Before Yield sec
28	3	0.041	113	21	0.041	34	5	0.070
30	3	0.051	114	21	0.057	35	5	0.040
100	3	0.047	75	50	0.057	36	5	0.058
			112	50	0.053	50	9	0.136
			78	80	0.046	38	10	0.059
			104	95	0.056	45	10	0.104
			108	95	0.047	46	10	0.043
			109	95	0.093	47	10	0.200
			102	100	0.140	48	10	0.052
			105	100	0.409*	52	10	0.049
			106	100	0.085	53	11	0.043
			107	103	0.392*	54	11	0.084
			122	103	0.337*	55	11	0.035
			110	105	0.364*	58	11	0.573*
						59	11	0.038
						61	11	0.036
						62	11	0.042
						64	11	0.036
						65	11	0.044
						68	12	0.085
						69	12	0.039
						44	12	0.576*
						72	13	0.595*
						73	13	0.427*
						40	15	0.464*
						41	15	0.522*

*Specimen did not yield.

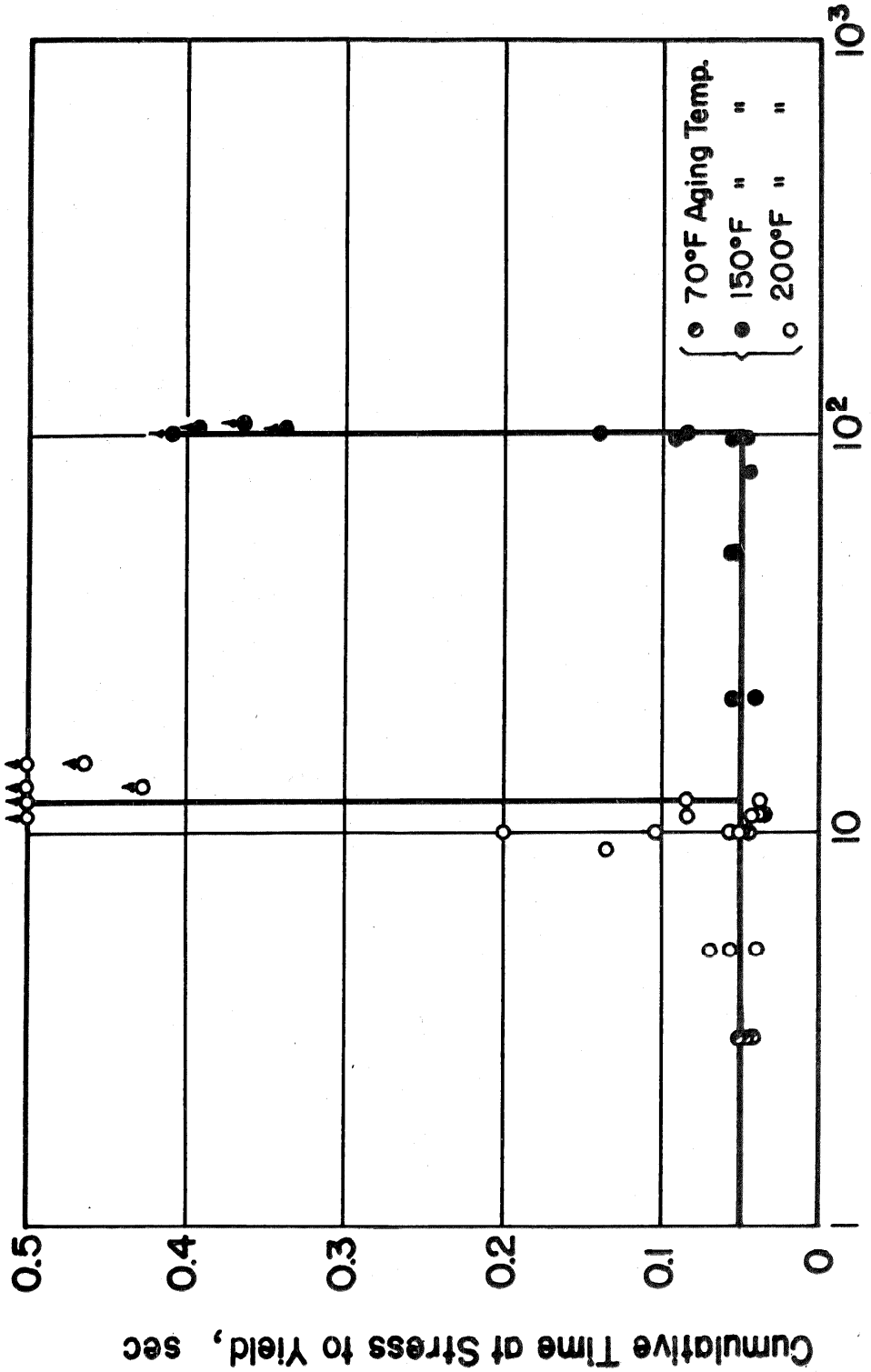

Fig. 10 Cumulative Time at Stress to Yield vs. Aging Time

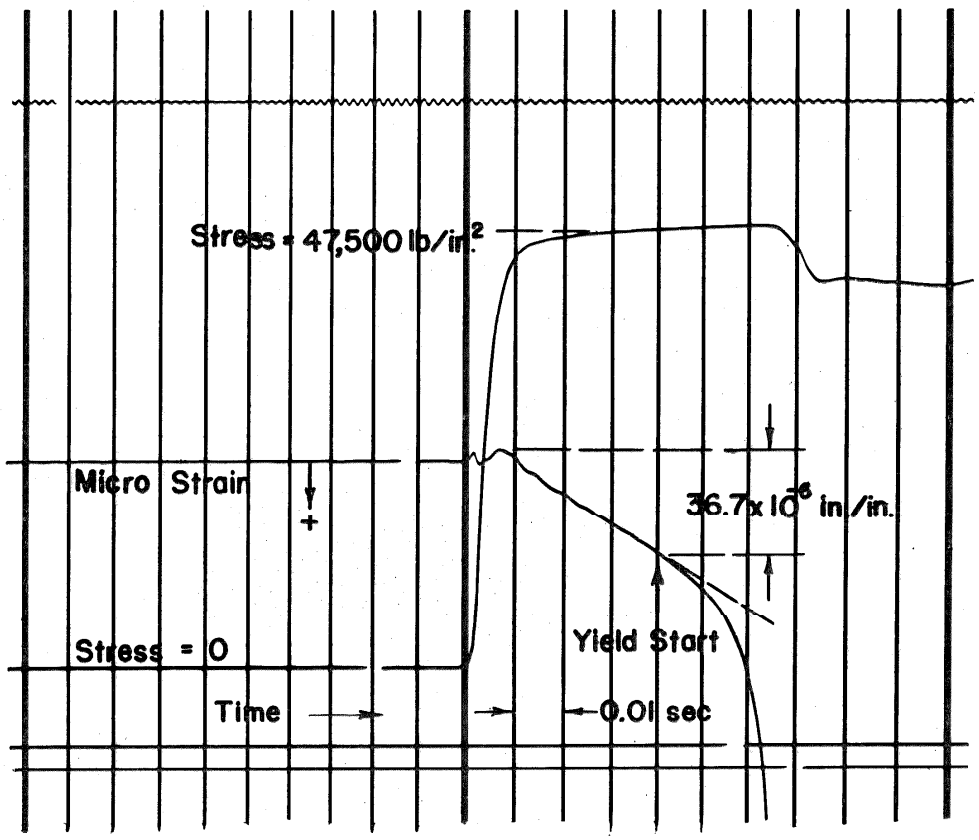

Fig. 11 Typical Record of Microstrain Under Constant Stress

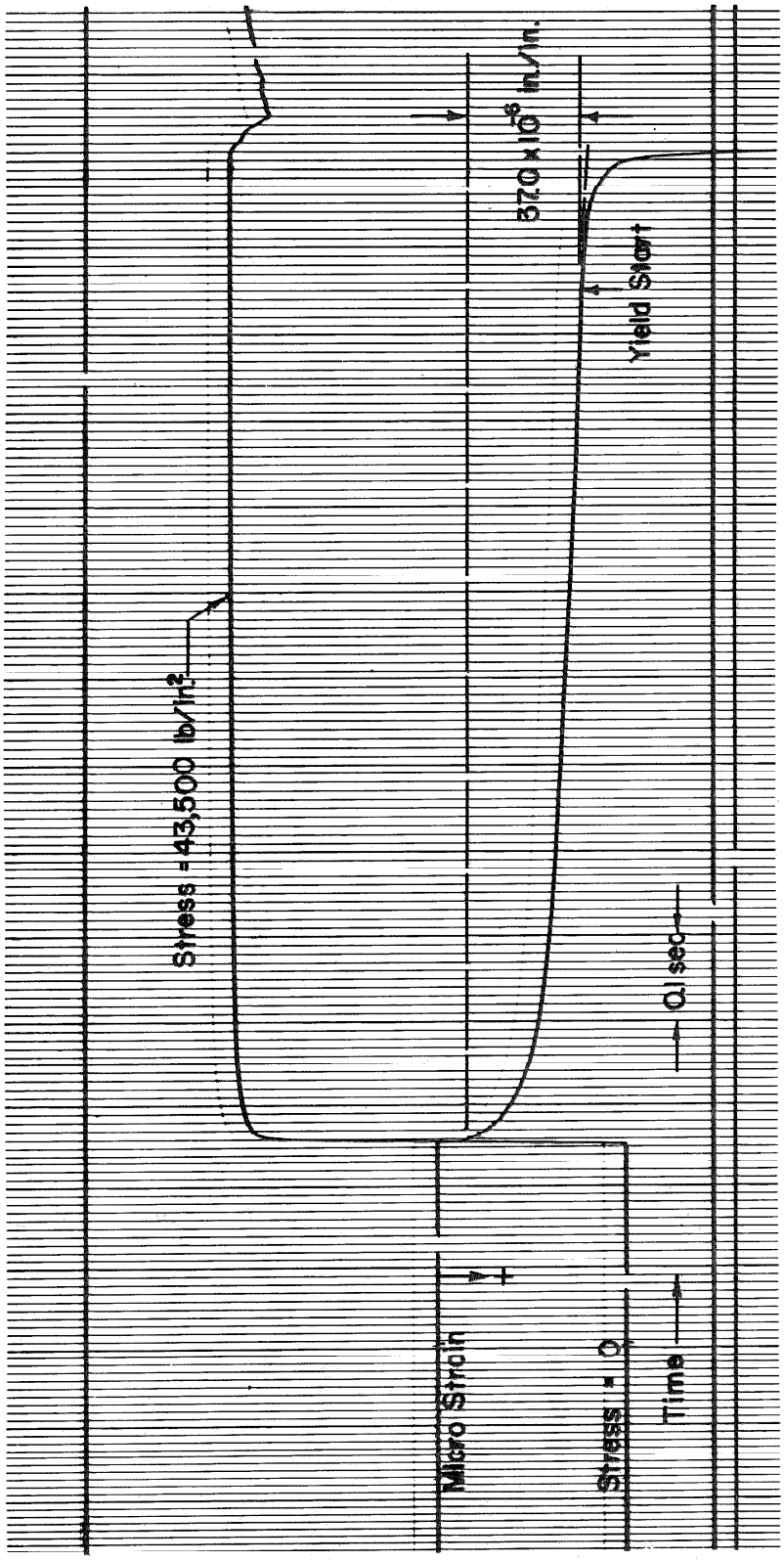

Fig. 12 Typical Record of Microstrain Under Constant Stress

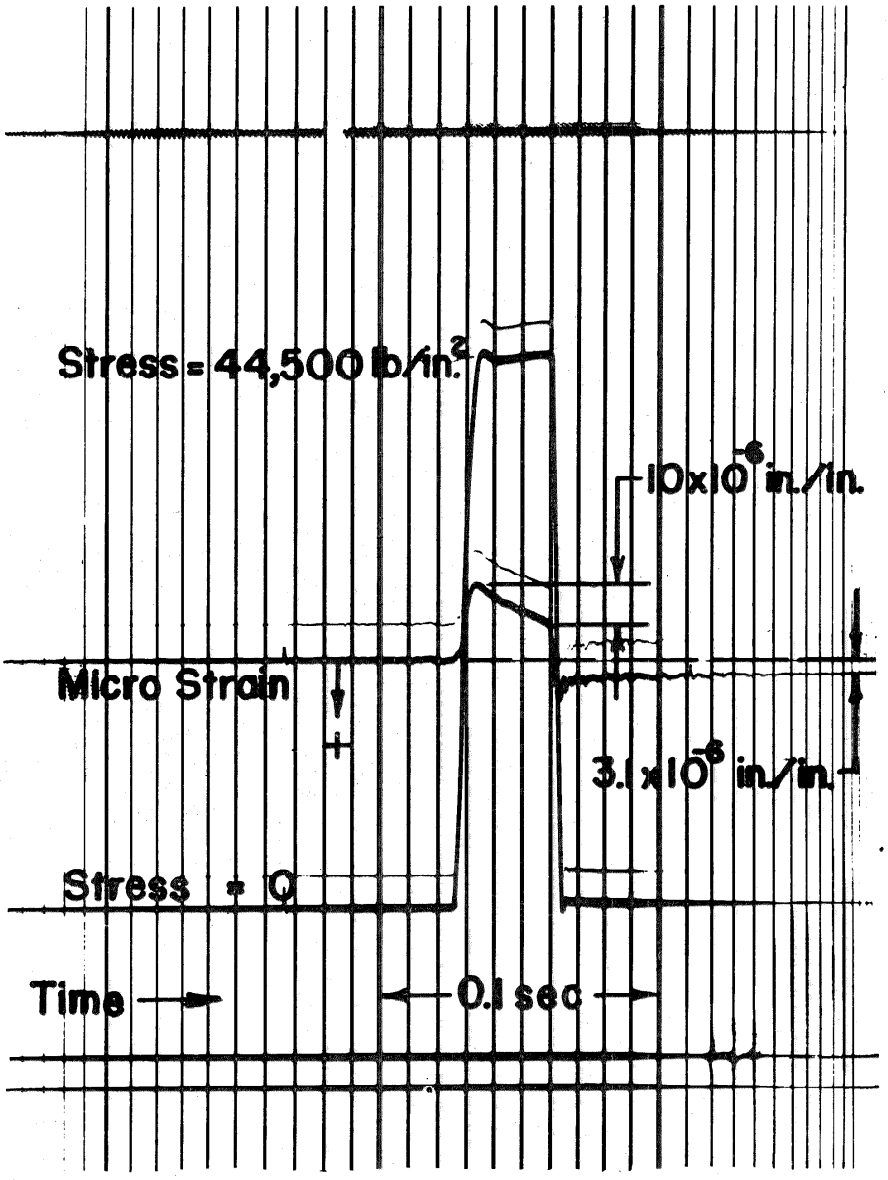

Fig. 13 Typical Record of Microstrain During Stress-Pulse

(2) A difference in sensitivities of the gages on the strain bar and the specimen.

(3) Misalignment between specimen and strain bar at the threaded connection which can result in a difference of the bending moment in the specimen and in the strain bar. This will result in bending strain inequality.

(4) A difference in Young's modulus between the X4130 strain bar and the test specimen.

These sources of elastic strain inequality do not produce any change in the indicated strain while the stress remains constant. Therefore, the changes of indicated strain which occur during the period of substantially constant stress may be attributed to plastic and anelastic microstrain in the specimen. The microstrain shown in the records is indicated by a downward deflection of the trace, whereas an unbalanced elastic strain may deflect the trace in either direction. This explains the difference in the direction of deflection at the beginning of the strain trace in Figs. 12 and 13. The strain which is indicated on the record during the period of stress rise is subtracted from the total indicated strain; thus, any microstrain occurring during the period of stress rise is neglected.

Anelastic and plastic strains which may occur in the strain bar also introduce a subtractive error. Hence, the measured microstrain is always less than the true plastic and anelastic microstrain in the specimen. Although it is difficult to make a reliable estimate of the total error due to these effects, there is some justification for believing that it is small. First, the strain correction for elastic

unbalance is normally a small portion of the indicated microstrain during the entire record. This provides an indication that the microstrain which may occur during the period of stress rise is small compared to the total microstrain. Second, the stress in the strain bar is approximately one fourth the value of the yield stress for this material; therefore, the anelastic and plastic strain in it should be negligible.

The total microstrain before yielding for various stresses above the static upper yield stress in rapid-load and stress-pulse tests is given in Table IV. A mean value of microstrain of 30×10^{-6} in./in. was found to take place prior to yielding in ten tests at various stresses. Although the microstrain varied from 20×10^{-6} in./in. to 37×10^{-6} in./in. in these tests, there is no systematic correlation with the magnitude of the stress. The microstrain rate during each test decreases with time until yielding starts. A recovery of approximately 50 per cent of the microstrain was observed when the stress was removed as illustrated in Fig. 13. Successive stress-pulse and aging cycles showed decreasing amounts of microstrain in each stress-pulse cycle. When the aging conditions induced recovery, the decrease in microstrain for successive stress-pulse aging cycles was greater.

The total microstrain (equilibrium microstrain) for various stresses below the static upper yield stress is given in Table IV. Microstrain vs. time relations for a series of rapidly applied constant stresses are presented in Fig. 14.

The distribution of the microstrain over the specimen gage length was investigated. The difference in strain between two regions of the gage section was measured by means of four type A-8, SR-4 strain gages.

Table IV

MICROSTRAIN BEFORE YIELDING
FOR VARIOUS STRESSES AND STRESS-PULSE CYCLES

Annealed Material

Rapidly Applied Constant Stress
Greater Than the Yield Stress

Specimen Number	Stress 10^3 lb/in.^{2}	Microstrain Prior to Yield 10^{-6} in./in.
198	49.4	26.8
200	47.5	36.7
193	46.5	29.0
189	46.0	32.9
192	46.0	28.0
190	45.5	20.0
202	44.5	35.3
203	43.6	37.0

15 min Aging at 70°F Between Stress-Pulses

Specimen Number	Stress 10^3 lb/in.^{2}	Duration of Pulses sec	Microstrain Prior to Yield 10^{-6} in./in.	
194	45.0	0.045	26.5	- Yield During 3rd Pulse
196	44.0	0.041	28.0	- Yield During 13th Pulse

Annealed and Homogenized Material

Rapidly Applied Constant Stress
Less Than the Yield Stress

Specimen Number	Stress 10^3 lb/in.^{2}	Equilibrium Microstrain 10^{-6} in./in.
19	25.0	3.0
18	29.0	4.0
20	31.5	6.0
21	35.5	10.0
17	38.5	13.0
15	41.0	21.5
16	41.0	24.0

103 min Aging at 150°F Between Stress-Pulses

Specimen Number	Stress 10^3 lb/in.^{2}	Duration of Pulses sec	Microstrain Prior to Yield 10^{-6} in./in.	
107	45.0	0.029	32.8	- No Yield in 14 Cycles
122	45.0	0.029	32.4	- No Yield in 12 Cycles

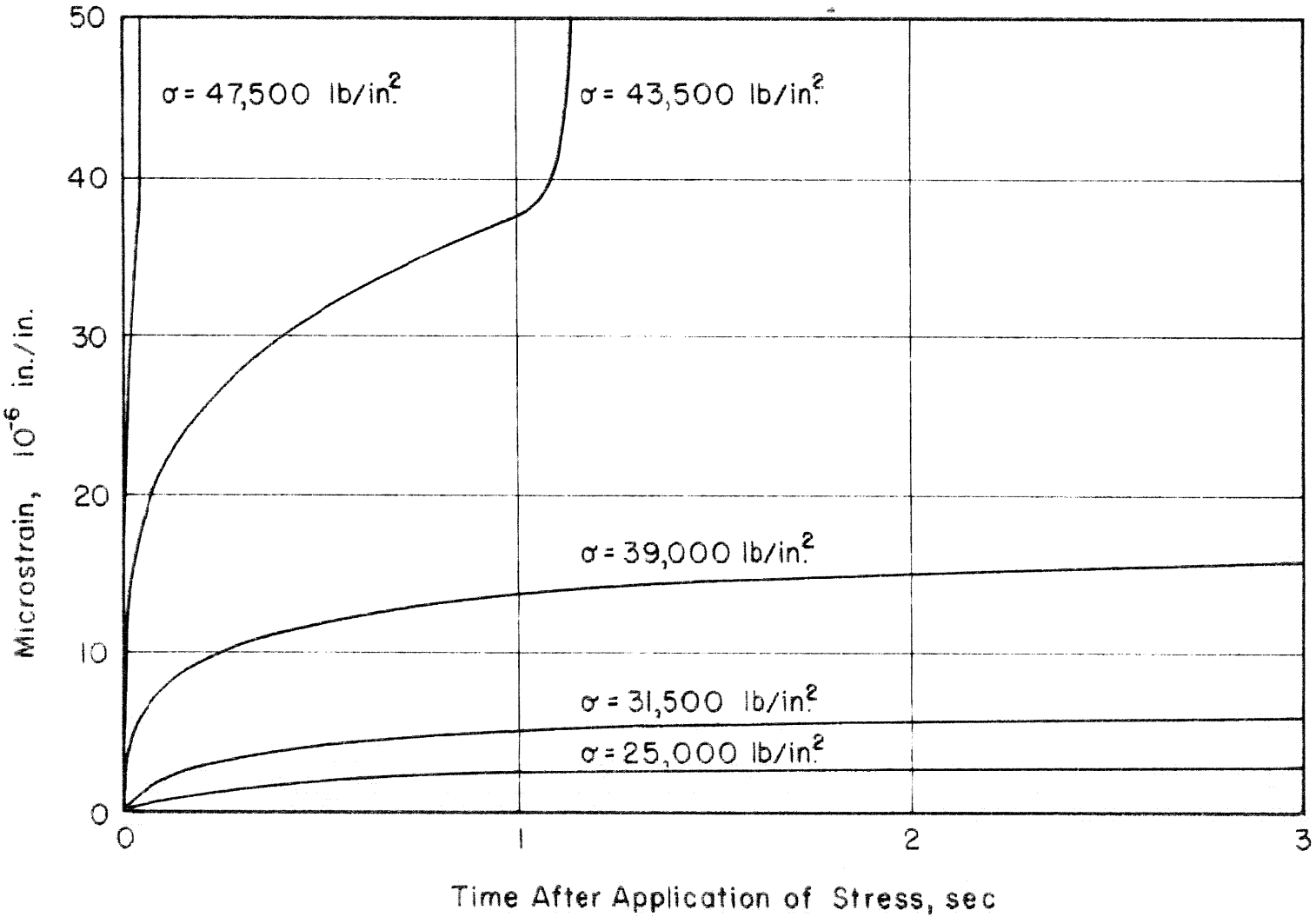

Fig. 14 Microstrain vs. Time for a Series of Constant Stresses

Two gages were bonded to each region, one on each side of the gage section, and the four gages were electrically connected so as to measure the strain difference between the two regions. These strain gages have a gage length of 1/8 in., and the specimen gage length is 1/2 in. The specimen was subjected to a rapid load, and the resulting test record, shown in Fig. 15, indicates no inhomogeneity in strain prior to the initiation of yielding. The elastic strain difference indicated during the period of increasing load is disregarded as in tests in which the strain bar is used. A second indication of the distribution of the microstrain was obtained in the following manner: The surface of a test specimen was mechanically polished, etched, and examined microscopically at magnifications of 100X and 600X between successive stress-pulses in an attempt to detect the formation of slip lines. No slip lines were observed until yielding took place during the third stress-pulse. Slip lines were then observed within the single Luder's band which had formed.

Tests on Material Previously Subjected to Stress-Pulse and Aging Cycles

The influence of stress-pulse and aging cycles on the static stress-strain relationship and on the stress-delay time relationship was investigated. Tests were conducted on specimens which did not yield in the stress-pulse and aging procedure because a sufficient aging period was given between stress-pulses to permit recovery.

The stress-strain relationships found in two static tests are plotted in Fig. 16. Table I gives the static upper and lower yield stress and yield strain for the original material and for the same material after being subjected to stress-pulse and aging cycles. The static upper and lower yield stress and the yield strain are not changed significantly by the stress-pulse and aging treatment.

The results of the stress-delay time determinations are given in Table II and plotted in Fig. 8. An increase in delay times by a factor of approximately four was found over the delay times for the original material for corresponding stresses.

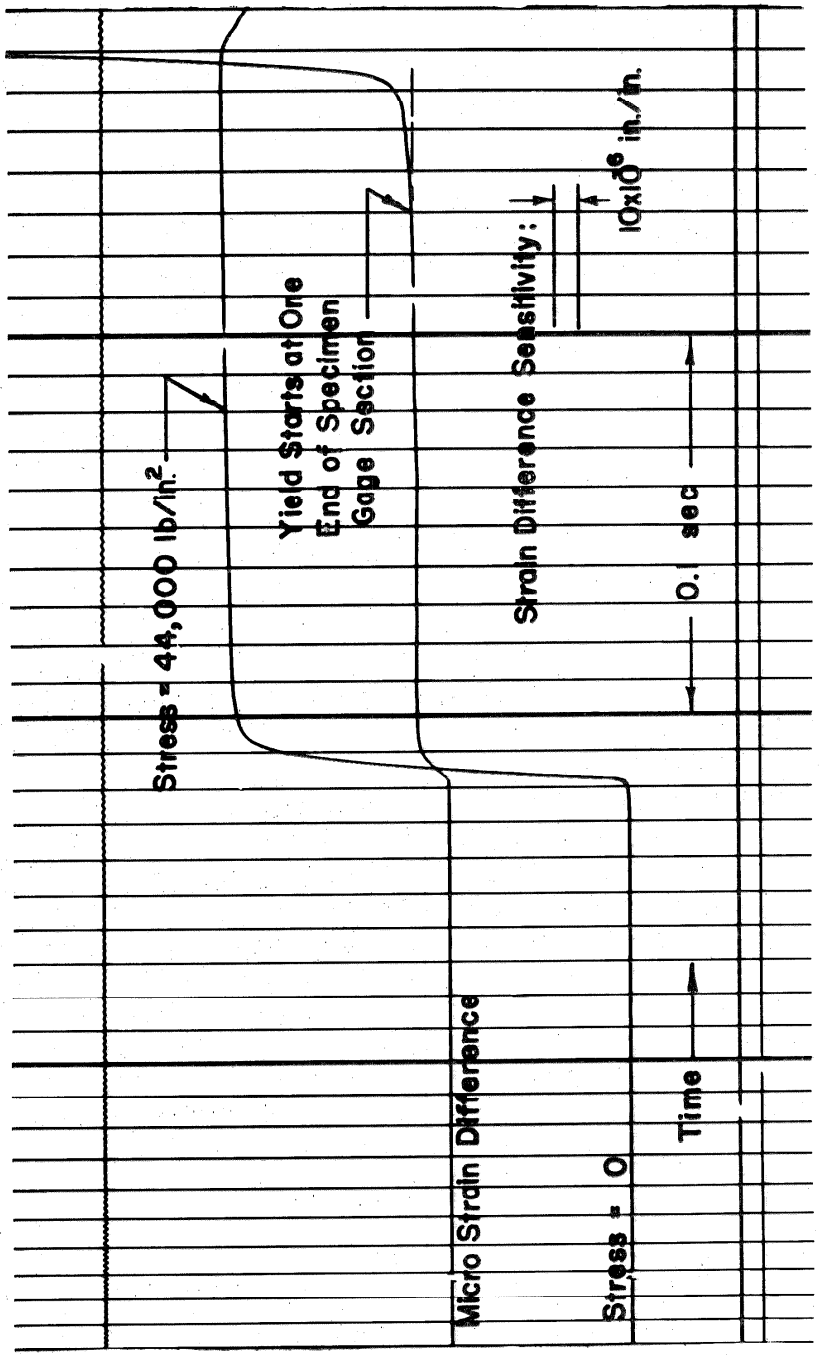

Fig. 15 Test Record of Distribution of Microstrain

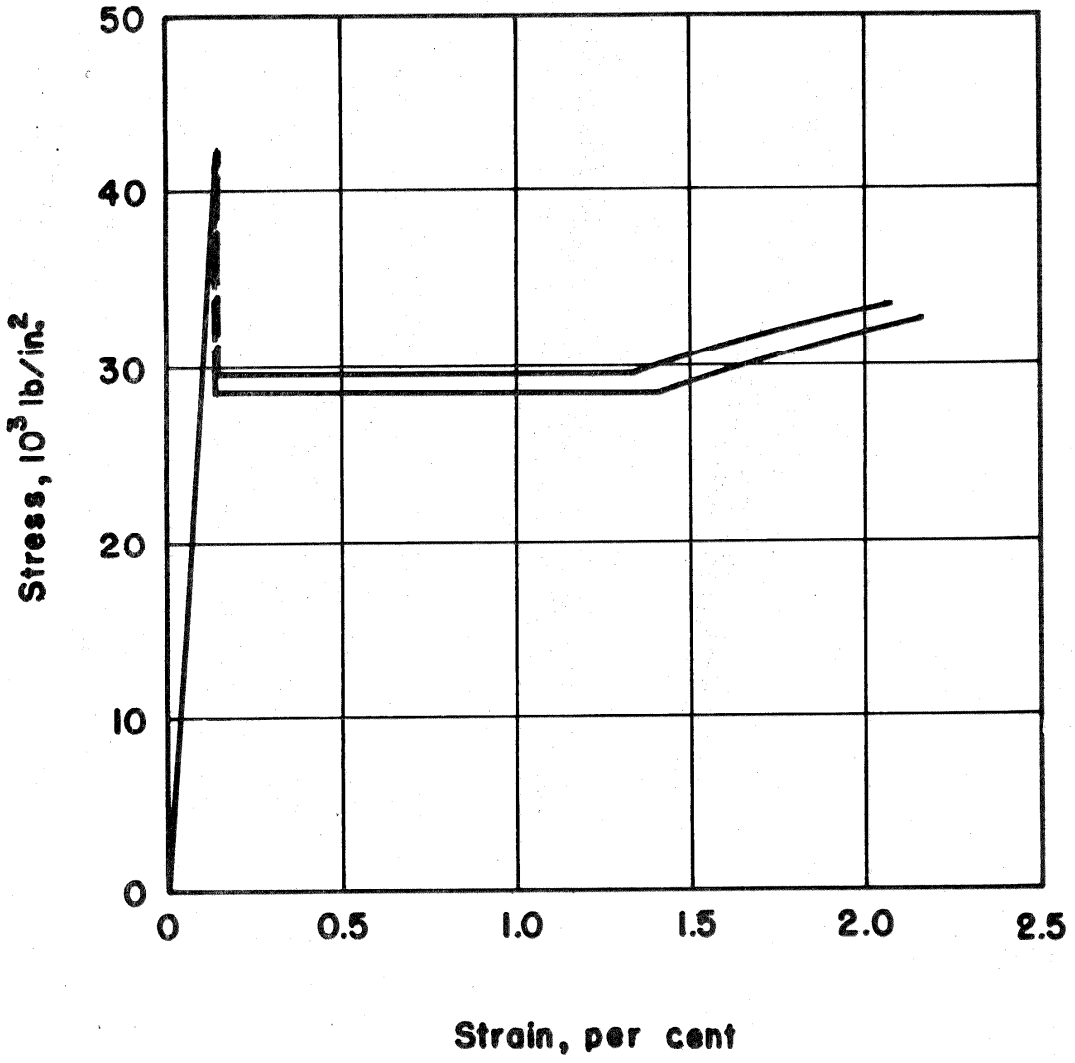

Fig. 16 Static Stress vs. Strain
Annealed and Homogenized Material
After Stress-Pulse and Aging Treatment

DISCUSSION OF EXPERIMENTAL RESULTS

The relations between stress and delay time for the annealed and homogenized material are given in Fig. 8. The stress-delay time relationship for the annealed material (14) is shown by a dashed line. The scatter in the data was found to be reduced by the homogenizing treatment. This treatment also produced changes in the stress-delay time relationship. The reduced scatter and the changes in the stress-delay time relationship can be attributed to a closer approach to the equilibrium state in the annealed and homogenized material. The amount of bending found in the rapid-load tensile tests is sufficient to introduce the scatter found in the stress-delay time determinations of the annealed and homogenized material.

The results of the repeated stress-pulse tests presented in Fig. 10 show that a definite recovery from the effects of the previous stress-pulse takes place when the time and temperature between stress-pulses is sufficient. An activation energy for the recovery process can be found by assuming that the recovery follows a law of the form

$$t \text{ proportional to } e^{Q/RT}$$

where t is the critical aging time for recovery,

Q is the activation energy of the recovery process,

R is the gas constant, and

T is the absolute aging temperature.

The recovery times of 12 min at 200°F and 100 min at 150°F give an activation energy of 18,300 cal/mole for the recovery process. There is an uncertainty of 10 per cent in this value due to scatter in

the critical aging time and the fluctuation of the aging temperature. This activation energy corresponds to the activation energy of strain aging (1), (2), (8), (18,100 cal/mole), and to the activation energy of the diffusion of carbon and nitrogen in alpha iron (carbon: 18,100 cal/mole (16), 19,800 cal/mole (17); nitrogen: 17,700 cal/mole (17)). Thus, it is reasonable to assume that the mechanism of recovery from previous stress-pulses is related to the mechanism of strain aging and to the diffusion of carbon and nitrogen in the steel.

The recovery phenomenon may be due to the stabilization of dislocations which have been moved by the stress-pulses. The theory of Cottrell and Bilby (9) for the formation of an atmosphere of interstitial atoms at dislocation centers predicts that the fraction of a saturated atmosphere formed in a given time is

$$3\eta_o\lambda\left(\frac{\pi}{2}\right)^{\frac{1}{2}}(ADt/kT)^{\frac{3}{2}}$$

where t is the aging time,

η_o is the concentration of randomly dispersed solute, atoms/cm^3,

λ is the magnitude of the Burger's vector = 2.5×10^{-8} cm for alpha iron,

A is a constant related to the interaction energy between the solute atom and dislocation = 3×10^{-20} dyne/cm^2 (9),

D is the diffusion constant of solute atoms in the material,

k is Boltzmann's constant, and

T is the absolute temperature.

If sufficient recovery from previous stress-pulses to prevent yielding is assumed to take place when one half of a complete atmosphere

has formed, the critical aging time for recovery should be

$$t = \frac{(0.5)^{\frac{3}{2}} k T}{A D (3 \eta_o \lambda)^{\frac{3}{2}} (\frac{\pi}{2})^{\frac{1}{2}}} .$$

The solubility and diffusion constant for carbon over the range of aging temperatures used in this investigation are smaller than those for nitrogen, so it may be assumed that a nitrogen atmosphere forms. The diffusion constant for nitrogen in alpha iron is taken from Wert and Zener (17). The solubility of nitrogen in iron is taken from an extrapolation of Dijkstra's measurements (18). Calculated and experimental values of recovery times are given below for aging temperatures of 150°F and 200°F.

Aging Temperature	D cm^2/sec	η_o $atoms/cm^3$	Recovery Time	
			Calculated	Experimental
150°F	5.05×10^{-15}	4.09×10^{17}	270 min	100 min
200°F	3.74×10^{-14}	8.53×10^{17}	13 min	12 min

The difference between the calculated and experimental recovery times may arise from inexact values of A, D, and η_o, and from the fact that the contribution from carbon diffusion is neglected. Thus, it seems probable that the Cottrell and Bilby theory is substantially correct for describing the process of recovery of low-carbon steel from the effects of stress-pulses.

A microstrain of approximately 30×10^{-6} in./in. was measured prior to yielding for both rapid loading and repeated stress-pulses when the test stress was greater than the yield stress. Although the microstrain varied from 20×10^{-6} in./in. to 37×10^{-6} in./in., there is no systematic correlation with the magnitude of the stress. No nonuniformity

in microstrain was found over the specimen gage section prior to yielding. This indicates that the microstrain does not result from the progressive formation of the Luder's band which appears on yielding. The total microstrain before yielding for test stresses greater than the yield stress agrees in order of magnitude with that found by Averbach (19) (50 - 60 x 10^{-6} in./in.) in static tests on polycrystalline samples of iron and steel. Experimental microstrain vs. time relations for several test stresses are presented in Fig. 14. The strain rate decreases with time when the test stress is less than the yield stress. When the test stress exceeds the yield stress, the strain rate decreases with time until the initiation of yielding, which is characterized by an increase in strain rate. The final values of microstrain (equilibrium strain) for the series of tests in which the stress was less than the yield stress are shown by the points plotted in Fig. 17.

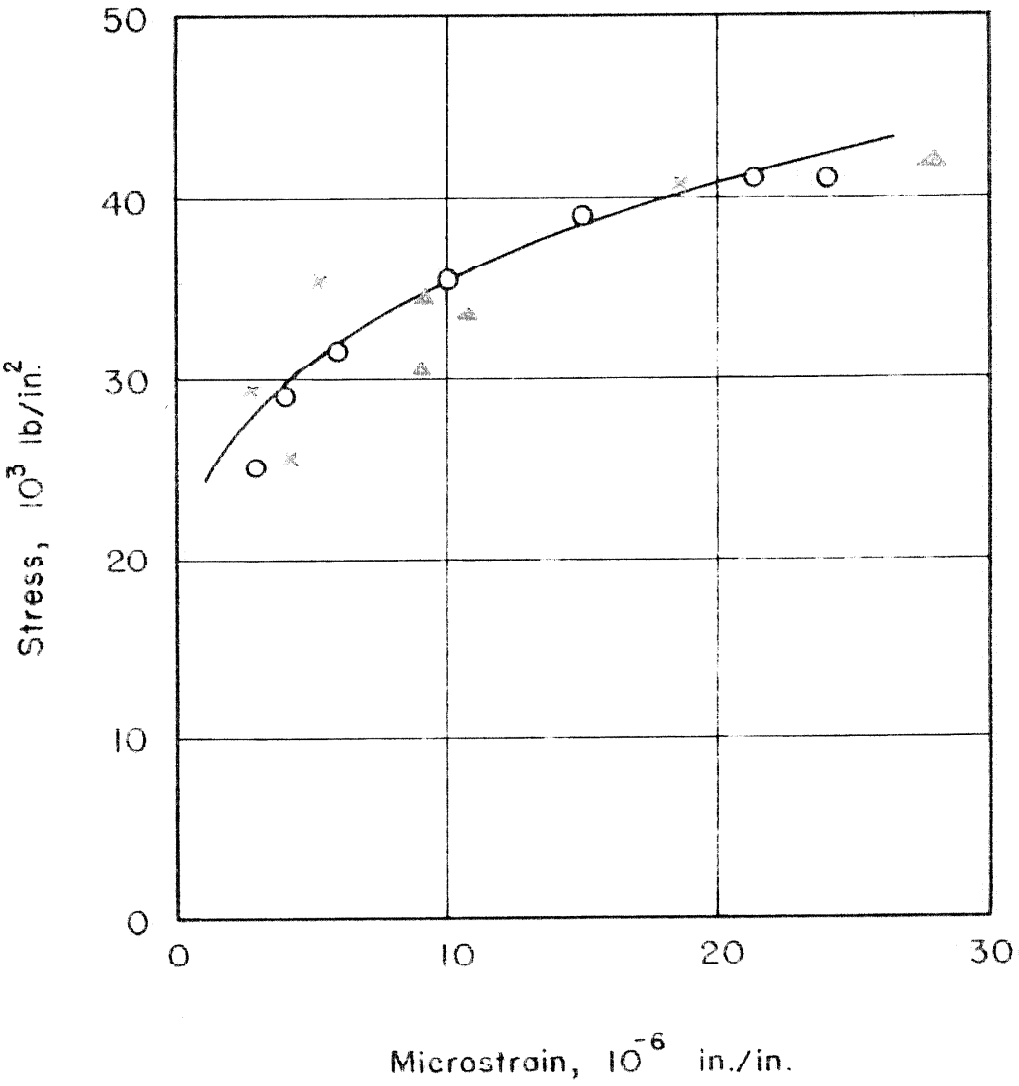

Fig. 17 Stress vs. Equilibrium Microstrain, [illegible]

[illegible]

THEORETICAL DISCUSSION

The concepts of the theory of dislocations will be examined in order to determine whether or not they can explain the experimental observations of this investigation. To date, the treatment of the strain produced by the action of dislocations in low-carbon steel has been qualitative in nature. The quantitative experimental evidence presented in this thesis provides a basis for an evaluation of the present theories.

A. H. Cottrell (7) has recently presented some promising additions to the previous concept of the mechanism for the initiation of yielding in polycrystalline low-carbon steel. He extends the previous theory of dislocations, anchored by interstitial solute atoms, to include the following concepts:

(1) Releasing a dislocation from a grain boundary requires a larger force than releasing an anchored dislocation within a crystal.

(2) A few dislocations are released prior to yielding, and their movement is obstructed by interaction with other nearby anchored dislocations or grain boundaries. Yielding is not initiated until the resistance offered by obstructions to the movement of dislocations is overcome.

An anchored dislocation within a crystal may move when its total energy is greater than the potential energy of the anchoring barrier. For a given stress, the number of dislocations which can move in a given time is determined by the statistics of the fluctuations

in thermal energy of the dislocations. Therefore, a definite period of time would be required for a particular stress to release a given number of dislocations. When a sufficient number of dislocations are released and move to an opposing obstruction, they may overcome the restraint offered by the obstruction and initiate an avalanche of dislocations which results in yielding. The delayed yield phenomenon may be qualitatively explained by this mechanism. Furthermore, the relatively constant value of microstrain observed before yielding at stresses exceeding the yield stress can also be qualitatively explained by these concepts. The temperature dependence of the delay time will, by Cottrell's theory, depend upon two factors:

(1) The temperature dependence of the rate at which dislocations are released from within a grain, and

(2) The temperature dependence of the strength of the obstructions which impede the motion of the released dislocations. This is indicated experimentally by the temperature dependence of the upper yield stress.

Both of these effects contribute to the decrease in delay time for yielding as the temperature is increased, which is observed experimentally (15).

A recent theory by Holden (20) attributes the yield behavior of single crystals of iron to a dislocation-collision process wherein moving dislocations free stationary dislocations by an interchange of energy. The result of such a process could only give rise to a strain rate that increases with time for a constant stress. This is contrary to the experimental observations of this investigation on polycrystalline

material. Thus, the theory of Cottrell appears to be more suitable for an explanation of the present experimental observations.

The decreasing microstrain rate observed in this study might be attributed to a depletion of the reservoir of dislocations which can be moved by the applied stress. The relation

$$\dot{\varepsilon} = \varepsilon_o - K\varepsilon$$

would be predicted by this hypothesis where

K and ε_o are constant for a given stress and temperature,

$\dot{\varepsilon}$ is the strain rate, and

ε is the strain.

Experimental strain rate vs. strain for various stresses is presented in Fig. 18. The strain rate is not a linear function of strain as is predicted by a depletion mechanism. This indicates that some other mechanism gives rise to the observed strain rate vs. strain relations.

A mechanism has been proposed by Frank and Read (21) that may explain the observed microstrain. They have postulated a multiplication process for slow-moving dislocations which in effect constitutes a dislocation source. The process is illustrated in Fig. 19. The segment BC of a dislocation loop ABC lies in the active slip plane, DEFG; other parts of the loop lie outside of the plane so that the points B and C are fixed. A suitable applied shear stress will cause the segment BC to curve and generate new dislocation loops as shown. The stress required to form a new dislocation loop without the aid of thermal fluctuations is

$$\tau_c = \frac{G\lambda\alpha}{\ell} \qquad (1)$$

where τ_c is the resolved shear stress,

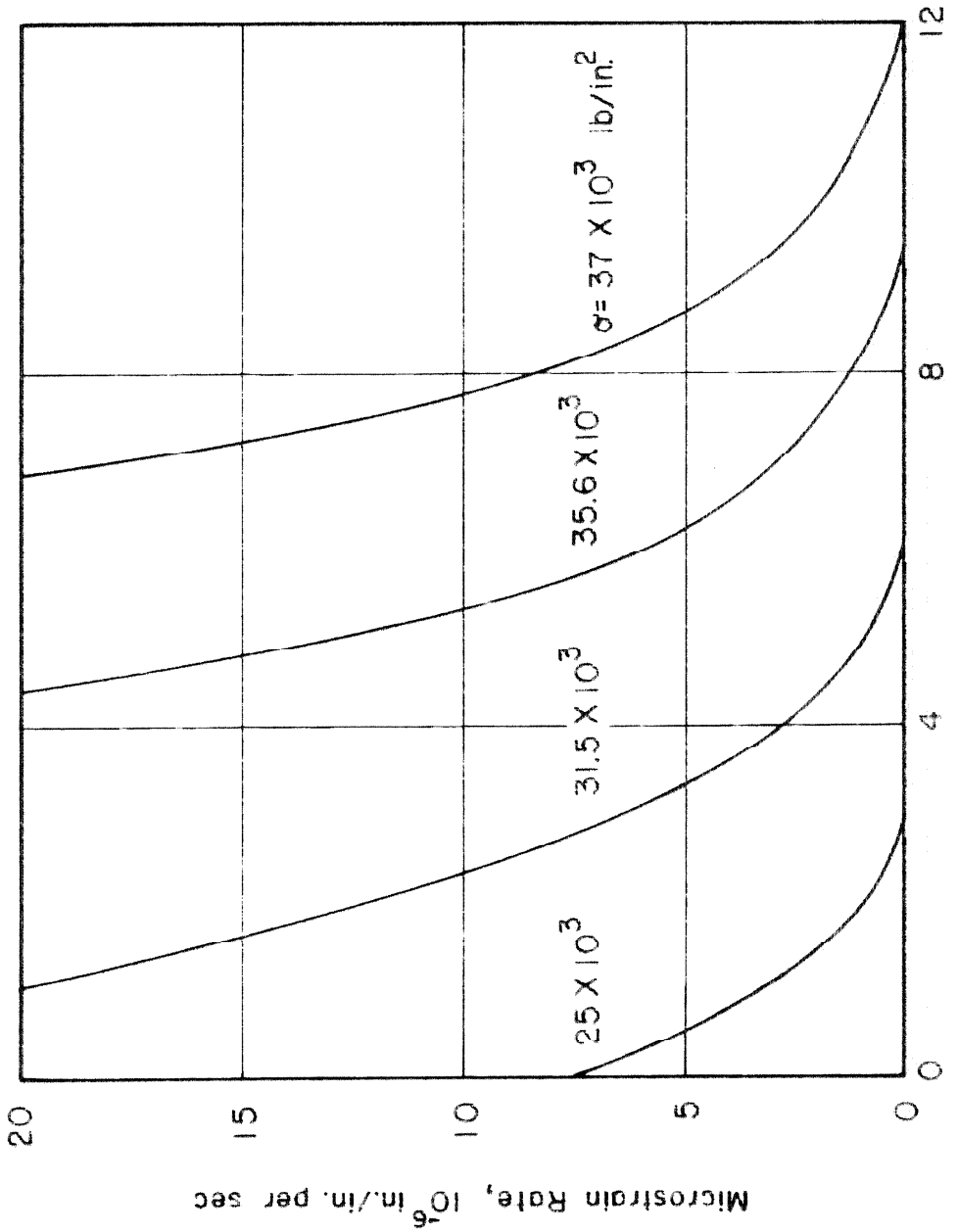

Fig. 18 Microstrain Rate vs. Microstrain for a Series of Constant Stresses

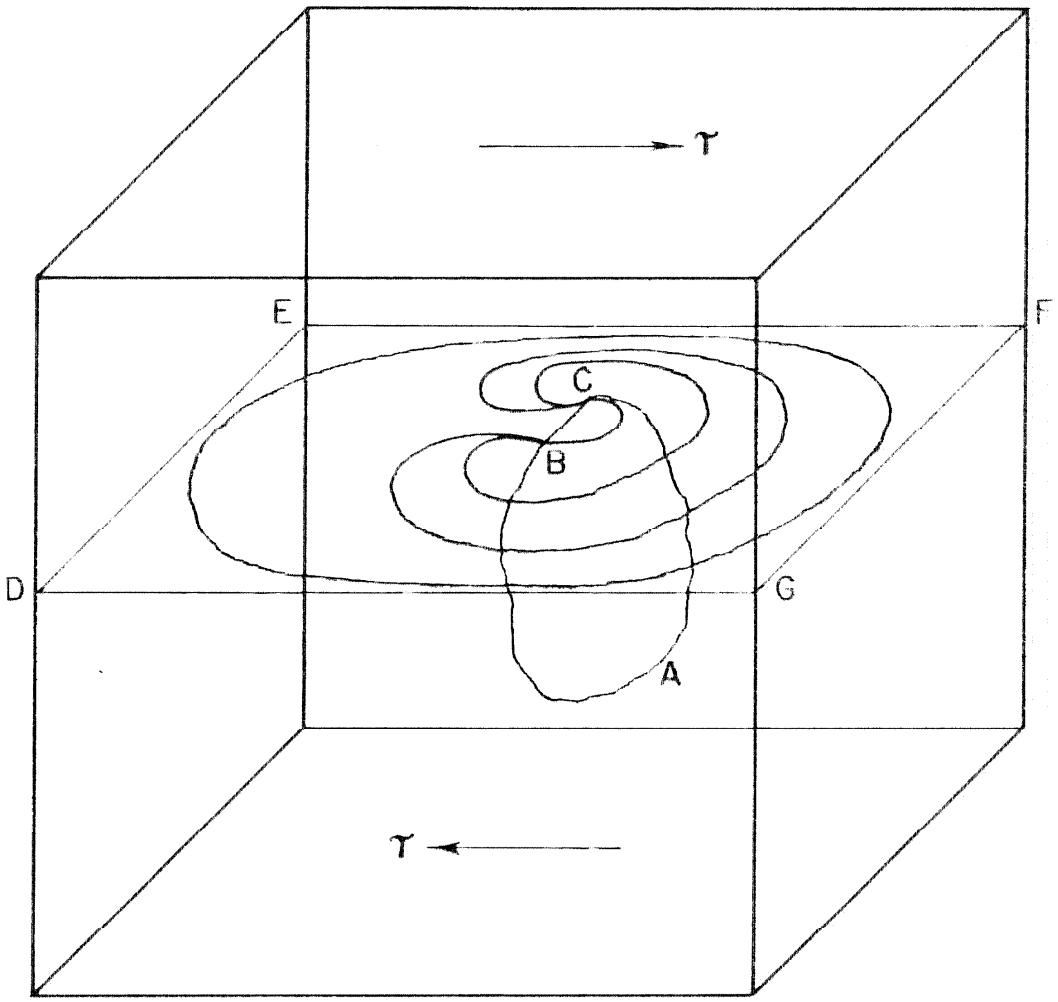

Fig. 19 Frank-Read Dislocation Source

α is a constant of the order of unity,

G is the shear modulus, and

ℓ is the original length of segment BC.

It may be assumed that initially the dislocations in annealed low-carbon steel all have complete atmospheres. As each successive loop is formed under the action of a stress, the original dislocation line is reformed, and must again escape from its atmosphere to form another loop.

The growth of the loops which have been formed will be stopped by obstructions, such as grain boundaries. The rate at which dislocations are generated by the Frank-Read source is a function of the applied stress. The local stress at the dislocation source is the sum of the applied stress and the stress field of opposite sign due to the array of previously released dislocation loops. Thus, the rate of generation of new dislocation loops will decrease as the number of previously generated loops increases. The decreasing microstrain rate observed in this study may be qualitatively explained by this mechanism. If the applied stress is low enough, the generation of new dislocation loops will be stopped completely before a sufficient number have been formed to break through the grain boundaries or other obstructions. The equilibrium microstrain observed in the experiments in which the test stress was less than the yield stress would then correspond to the total strain produced by the dislocation sources when the generation of new dislocation loops is stopped.

The equilibrium microstrain produced by Frank-Read sources distributed throughout the material will now be calculated. The properties of an individual dislocation source will first be determined, and then microstrain produced by a distribution of sources throughout the material will be considered. The microstrain is a function of the number

of dislocation loops formed, and the distance that they have moved.

Dislocation loops may pass through some obstructions, such as dislocation lines which intersect the slip plane of the loop, inclusions, and foreign atoms by a process similar to the formation of a dislocation loop. Thus, the obstructions which stop the motion of dislocation loops may be considered to be grain boundaries.

A Frank-Read source which has formed a number of dislocation loops in a particular slip plane is schematically illustrated in Fig. 20. The stress field associated with a short segment of a dislocation loop is very complex. However, the stress field associated with a straight dislocation line of infinite length has been given by Koehler (22). The mathematical development of the theory is made possible if the interaction between opposite sides of dislocation loops is neglected, and an equilibrium array of straight, parallel, dislocation lines of infinite length is considered. The radial spacings between the dislocation loops and the source are assumed to be equal to the equilibrium spacings between infinite dislocation lines and a single dislocation line which represents the source. The minimum distance between the dislocation source and the grain boundary along the slip plane is taken to be 2L, as indicated in Fig. 20. The dislocation model is shown in Fig. 21a, where x is a distance in units of L along the shortest line between the source and grain boundary in the slip plane. The interaction between a dislocation and a grain boundary is not known. It will be assumed that the grain boundary cannot move and that it may be represented as a single dislocation line.

The stress at a point x associated with an infinite dislocation line at x_1 is given by

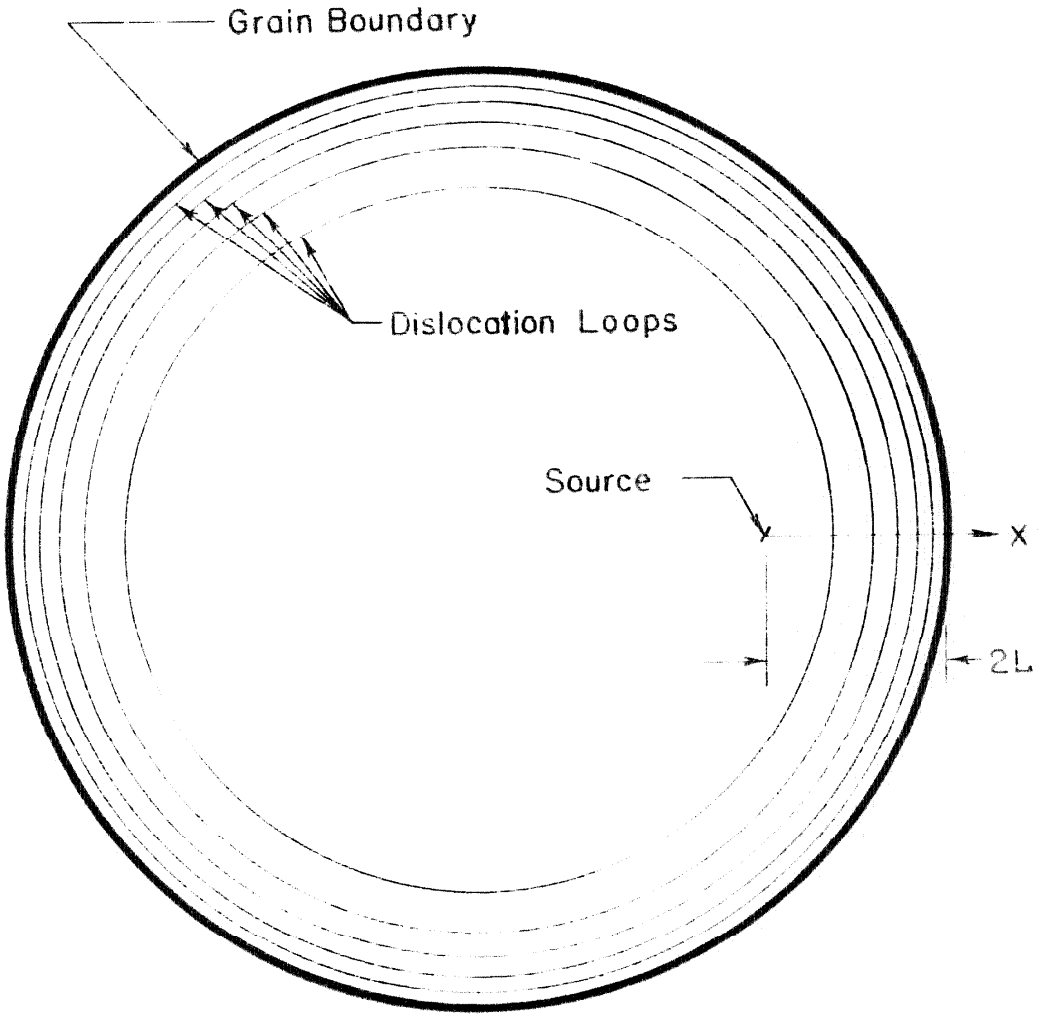

Fig. 20 Schematic Representation of a Dislocation Source and Dislocation Loops on a Slip Plane

$$\tau = \frac{B}{L(x-x_1)} \qquad (2)$$

where τ is the shear stress at point x,

$B = \frac{G\lambda}{2\pi(1-\nu)}$ for a positive edge-type dislocation, and

ν is Poisson's ratio.

It is convenient to use a dimensionless stress ratio, $P = \frac{\tau L}{B}$, in the calculations. The main contributions to the stress at a point between the dislocation source and the grain boundary are the applied stress and the stress due to the nearest dislocations. The stress due to dislocations on the opposite side of the source is comparatively small and may be neglected.

Eshelby, Frank, and Nabarro (23) have developed a mathematical method for determining the equilibrium positions of dislocations in linear arrays. They discuss the dislocation model of Fig. 21b for the case with no applied stress. A general solution is not given for the equilibrium positions of the dislocations with an applied stress. The treatment of this case by the method of Eshelby, Frank, and Nabarro is not practical when a general solution is desired.

The use of an electrostatic analogy to establish the properties of the dislocation model is helpful. This is possible since the force potential associated with a line charge and the stress potential associated with a line dislocation are both logarithmic. The difficulties encountered in the method of Eshelby, Frank, and Nabarro may be eliminated if n dislocations between the source and grain boundary are considered

to be continuously distributed. The number of dislocations between the source and grain boundary is assumed to be sufficiently large such that they may be represented by a continuous distribution. The electrostatic model is shown in Fig. 21b, where the two line charges with strength Q_o per unit length, at $x = \pm a$, represent the source and grain boundary. An infinitely long, thin, conducting strip with charge nQ_o per unit length is placed between the two line charges, and represents n dislocations on the slip plane between the source and grain boundary. A uniform field, E_o, represents the resolved shear stress ratio, P_o, in the dislocation model. The charge distribution across the strip is then analogous to the dislocation distribution between the source and grain boundary. The line charges must be separated from the strip by a small distance, δ, such that there will be no transfer of charge between them. Thus,

$$a = 1 + \delta, \text{ where}$$

$$\delta << 1.$$

The charge distribution across the strip is found by the use of a complex potential. The method given in Smythe (24) is used. The potential for the electrostatic model, Fig. 21b in the z plane, is found from the potential for a charged, conducting cylinder and two line charges, as shown in Fig. 21c in the z_1 plane. A transformation which maps the z_1 plane to the z plane gives the potential for the electrostatic dislocation model.

The complex potential for an infinite cylinder between two line charges in a uniform field $E_o/2$, Fig. 21c, is found by the method of images to be

$$W(z_1) = -\frac{E_o}{2}\left(z_1 - \frac{1}{z_1}\right) - 2Q_o\left[(z+n)\ln z_1 - \ln\frac{z_1 - \frac{1}{a}}{z_1 - a} - \ln\frac{z_1 + \frac{1}{a}}{z_1 + a}\right]. \qquad (3)$$

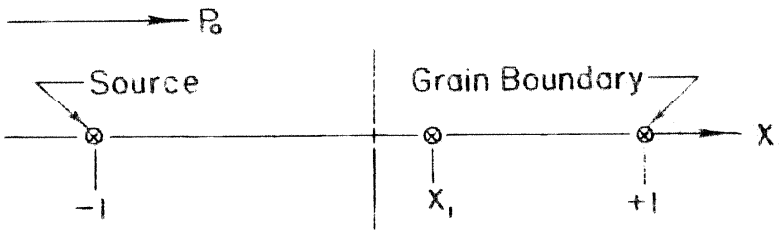

Fig. 21a Dislocation Model

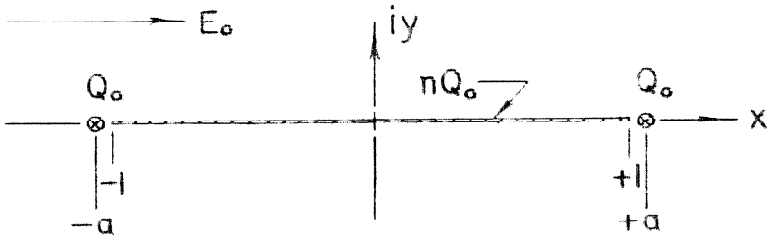

Fig. 21b Electrostatic Model, z Plane

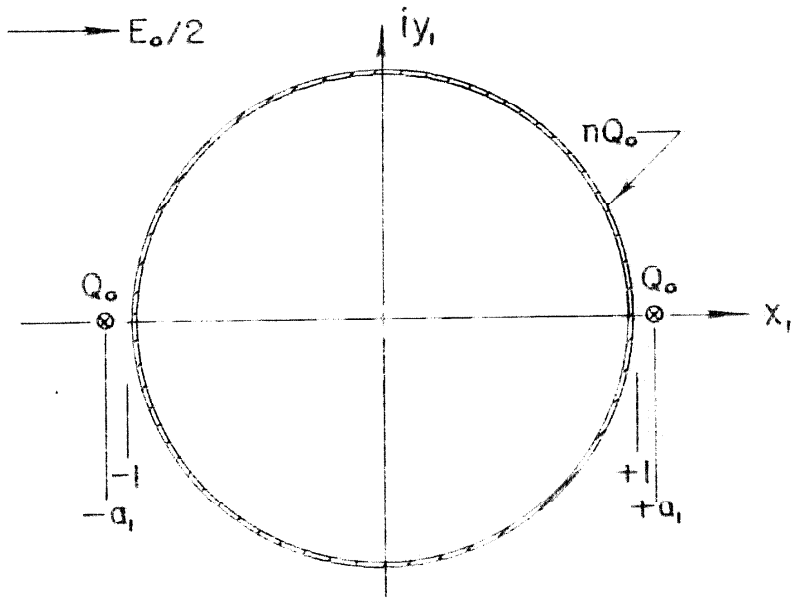

Fig. 21c Electrostatic Model, z_1 plane

The complex potential for the electrostatic dislocation model in the z plane is found from equation 3 by the transformation $z_1 = z - \sqrt{z^2-1}$ and is

$$W(z) = -E_0\sqrt{z^2-1} + 2Q_0\left[\ln\frac{z-a-\sqrt{z^2-1}+\sqrt{a^2-1}}{z-a-\sqrt{z^2-1}-\sqrt{a^2-1}}\right. \tag{4}$$

$$\left. + \ln\frac{z+a-\sqrt{z^2-1}-\sqrt{a^2-1}}{z+a-\sqrt{z^2-1}+\sqrt{a^2-1}} + (n+2)\ln\left(z-\sqrt{z^2-1}\right)\right].$$

The number of dislocations produced by a dislocation source may be estimated by use of the electrostatic analogy. The Frank-Read dislocation source will cease to generate new dislocations when the stress at the source is reduced below the value given by equation 1. The field at $x = -a$, exclusive of the field due to the line charge at that point, is

$$E(-a) = \frac{E_0 a}{\sqrt{a^2-1}} + \frac{2Q_0}{\sqrt{a^2-1}}\left(\frac{\sqrt{a^2-1}}{2a} - 1 - n\right).$$

This is analogous to the stress ratio, $P(-a)$, at the dislocation source, exclusive of its own stress field. Thus,

$$P(-a) \cong \frac{P_0 a}{\sqrt{a^2-1}} + \frac{1}{2a} - \frac{1}{\sqrt{a^2-1}}(1+n) \tag{5}$$

since $\frac{E}{2Q_0}$ is analogous to P. Hence, the number of dislocations is

$$n \cong P_0 a - 1 + \frac{\sqrt{a^2-1}}{2a} - \sqrt{a^2-1}\,P(-a). \tag{6}$$

In the dislocation model, P(-a) is always less than P_o for n greater than zero. Therefore, the last term of equation 6 is small compared to the first term. Thus, the equilibrium number of dislocations produced by P_o is insensitive to P(-a) and is approximately

$$n \cong P_o - 1. \tag{7}$$

The charge between -1 and x on the strip is given by

$$Q(x) = \frac{1}{2\pi}\left[\operatorname{Im} W(x) - \operatorname{Im} W(-1)\right]$$

where Im W(x) and Im W(-1) are the imaginary parts of W(z) evaluated at z = x and z = -1. Thus,

$$\frac{Q(x)}{Q_o} = -\frac{E_o}{2Q_o\pi}\sqrt{1-x^2} + \frac{1}{\pi}\left[\tan^{-1}\frac{x-a-\sqrt{a^2-1}}{\sqrt{1-x^2}} - \tan^{-1}\frac{x-a+\sqrt{a^2-1}}{\sqrt{1-x^2}}\right.$$
$$\left. + \tan^{-1}\frac{x+a+\sqrt{a^2-1}}{\sqrt{1-x^2}} - \tan^{-1}\frac{x+a-\sqrt{a^2-1}}{\sqrt{1-x^2}} + (n+2)\sin^{-1}x\right] + \frac{n}{2} \tag{8}$$

where the principal values for the arctangent and the arcsine are taken in the first and fourth quadrants. The number of dislocations, n(x), between -1 and x is then

$$n(x) \cong -\frac{P_o\sqrt{1-x^2}}{\pi} + \frac{1}{\pi}\left[\tan^{-1}\frac{x-a-\sqrt{a^2-1}}{\sqrt{1-x^2}} - \tan^{-1}\frac{x-a+\sqrt{a^2-1}}{\sqrt{1-x^2}}\right.$$
$$\left. + \tan^{-1}\frac{x+a+\sqrt{a^2-1}}{\sqrt{1-x^2}} - \tan^{-1}\frac{x+a-\sqrt{a^2-1}}{\sqrt{1-x^2}} + (n+2)\sin^{-1}x\right] + \frac{n}{2} \tag{9}$$

since $\frac{Q(x)}{Q_o}$ is analogous to n(x). The center of gravity, x_m, of the distributed dislocations may be found by setting $n(x) = n/2$ in equation 9 and solving for x. Using equation 7,

$$\sqrt{1-x_m^2} \cong \left(1+\frac{1}{P_o}\right) \sin^{-1} x_m$$

since the arctangent terms may be neglected for x_m not near ±1. For P_o much greater than one,

$$\sqrt{1-x_m^2} \cong \sin^{-1} x_m \tag{10}$$

and the center of gravity is independent of the applied stress. Thus, the mean area of the dislocation loops (Fig. 20) is not a function P_o for P_o much greater than one.

The generation of one dislocation loop causes a relative displacement, λ, of the material above the area over which the dislocation loop has passed with respect to the material below. The displacement is in the slip direction. The mean displacement over a slip plane of unit area containing one dislocation loop is then

$$\lambda A$$

where A is the area swept out by the loop. The mean displacement when n loops are formed is

$$n\lambda A_m \tag{11}$$

where A_m is the mean loop area.

The above equations may now be used to estimate the equilibrium

microstrain as a function of tensile stress for a distribution of Frank-Read sources in polycrystalline material. The distribution of dislocation sources is assumed to be uniform and of density ρ_s per unit volume. For a fine grain polycrystalline material, such as that used in this investigation, the slip planes and slip directions may be assumed to be uniformly distributed over all possible angles. The fraction of the total number of dislocation sources which can generate dislocations on a given slip plane under the influence of the tensile stress is defined as $N(\ell)$ and is a function of the resolved shear stress on that slip plane. The resolved shear stress on a slip plane is given by

$$\tau = \frac{BP_o}{L} = \frac{\sigma}{2} \sin 2\beta \cos \varphi \tag{12}$$

where σ is the tensile stress,

β is the angle between the normal to the slip plane and the direction of tensile stress, and

φ is the angle between the maximum shear stress direction on the slip plane and the slip direction.

The number of sources per unit volume that will produce dislocation loops on slip planes which lie between β and $\beta + d\beta$, with slip directions between φ and $\varphi + d\varphi$, is given by

$$\frac{\rho_s N(\ell)}{4\pi^2} \, d\beta \, d\varphi .$$

The strain in the direction of the tensile stress produced by the mean displacement over one slip plane containing one dislocation source may be obtained from equations 7 and 11 and is given by

$$\lambda A_m (P_o - 1) \sin\beta \cos\beta \cos\varphi .$$

The equilibrium strain due to all dislocation sources on all slip planes is given by

$$\varepsilon \cong \frac{4\lambda\rho_s}{\pi^2} \int_{\varphi=0}^{\frac{\pi}{2}} \int_{\beta=0}^{\frac{\pi}{4}} A'_m [N(\ell)](P_o - 1) \sin 2\beta \cos\varphi \, d\beta \, d\varphi \qquad (13)$$

where A'_m is the mean dislocation loop area of all loops on all slip planes. For P_o much greater than one, A'_m is independent of P_o as indicated above. Thus,

$$\varepsilon \cong \frac{4\lambda\rho_s A'_m}{\pi^2} \int_{\varphi=0}^{\frac{\pi}{2}} \int_{\beta=0}^{\frac{\pi}{4}} [N(\ell)] P_o \sin 2\beta \cos\varphi \, d\beta \, d\varphi . \qquad (14)$$

In order to establish the validity of the assumption that P_o is much greater than one, the distribution, $n(\ell)$, of dislocation source lengths, ℓ, must be considered. This depends upon the configuration of dislocation loops in alpha iron which is not known. However, the configuration is probably related to a mosaic block structure within the crystals of metals. Such a block structure is believed to result from an array of dislocation loops. The maximum

length of dislocation lines on any slip plane may then correspond to the mosaic block size. Hence, it will be assumed that all dislocation sources have lengths less than some limiting value, ℓ_o . The form of the assumed distribution is

$$n(\ell) = C\left(1 - \frac{\ell^2}{\ell_o^2}\right) \qquad \text{for } \ell \text{ less than } \ell_o \text{, and}$$

$$n(\ell) = 0 \qquad \text{for } \ell \text{ greater than } \ell_o \text{,}$$

where c is a constant. The microstrain predicted by this distribution will be compared to the experimental equilibrium microstrain to determine whether or not the maximum dislocation length, ℓ_o , has any physical significance.

The fraction, $N(\ell)$, of the dislocation sources whose lengths are equal to or greater than ℓ , is then given by

$$N(\ell) = C\left[\left(1 - \frac{\ell}{\ell_o}\right) - \frac{1}{3}\left(1 - \frac{\ell^3}{\ell_o^3}\right)\right]. \tag{15}$$

Using equations 1, 12, and 15 in equation 14, and performing the integrations gives

$$\varepsilon \cong \frac{4\lambda\alpha}{3\pi\ell_o}(1-\nu)cL\rho_s A_m'\left(\frac{\ell_c}{\ell_o}\right)\left[\left\{3 + \frac{1}{2}\left(\frac{\ell_o}{\ell_c}\right)^2\right\}\cos^{-1}\frac{\ell_c}{\ell_o} - \frac{\ell_c}{\ell_o}\cosh^{-1}\frac{\ell_o}{\ell_c} - \frac{5}{2}\sqrt{\left(\frac{\ell_o}{\ell_c}\right)^2 - 1}\right] \tag{16}$$

where $\ell_c = 2G\lambda\alpha/\sigma$.

The quantity, ℓ_c, is the length of the shortest dislocation source which generates new dislocation loops under the action of the applied tensile stress, σ.

The constants ℓ_o and $cL\rho_s A'_m$ are chosen to fit the experimental data of stress vs. equilibrium microstrain, Table IV. The following values are taken as constants of the material:

$$\lambda = 0.985 \times 10^{-8} \text{ in.},$$

$$G = 11.6 \times 10^{6} \text{ lb/in.}^2,$$

$$\nu = 0.3, \text{ and}$$

$$\alpha = 1.$$

Equation 16 is plotted as a solid line in Fig. 17 for $cL\rho_s A'_m = 2.66$, and $\ell_o = 1.2 \times 10^{-5}$ in. which is 1.07×10^{3} times the lattice parameter of alpha iron. The experimental points are indicated by circles in the figure. Equation 16 follows the experimental data with the exception of the region of low stress, where the experimental strain is somewhat larger.

The assumed distribution is plotted in Fig. 22, as $n(\ell)/c$ vs. ℓ in lattice parameters. The quantity, ℓ_c, corresponding to the experimental yield stress, is indicated in the figure. Thus, a distribution of dislocation sources with lengths between ℓ_c and ℓ_o, as shown in Fig. 22, will produce a stress-microstrain relation similar to the experimentally observed relation. More microstrain would be produced in the region of low stress if a small fraction of the dislocation sources have lengths greater than ℓ_o, as indicated by the dashed line in Fig. 22. Such a distribution would predict a stress microstrain relation more nearly following the experimental points of Fig. 17.

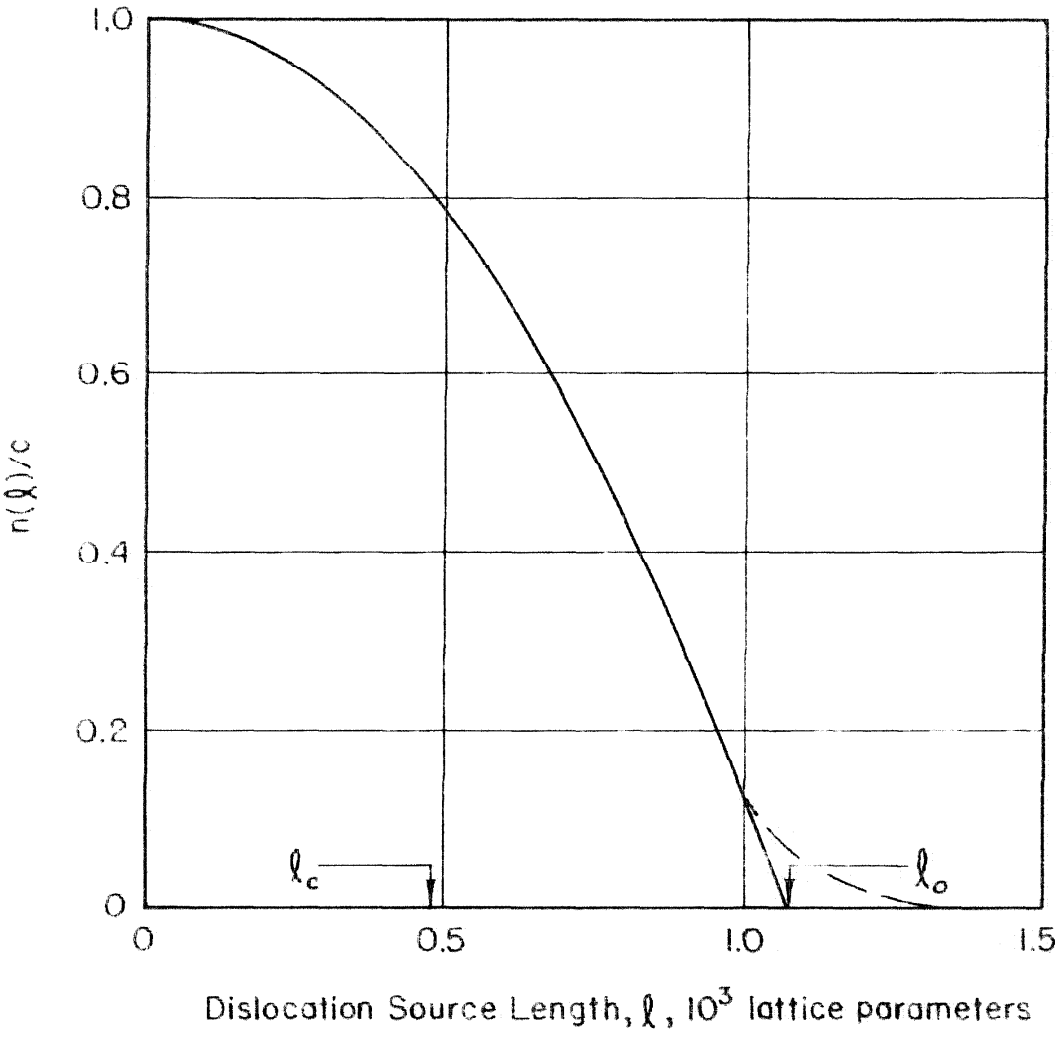

Fig. 22 Distribution of Dislocation Source Lengths

Some evidence exists to indicate that the value of the limiting length of dislocation source, ℓ_o, found above, is reasonable. A mosaic block size of approximately 10^3 lattice parameters is believed to exist (25) in crystals of alpha iron. The maximum length of dislocation lines on any slip plane may then be approximately 10^3 lattice parameters as is indicated by the value of the constant, ℓ_o.

The range of values of P_o which produces dislocation loops may now be calculated if it is assumed that grain boundaries are the obstructions which stop the motion of the loops. The range of P_o will be estimated assuming spherical grains. The mean distance between a point inside a grain and the nearest grain boundary, along a slip plane, is approximately 0.13 D where D is the diameter of the grain. Thus, the mean value of L is approximately 0.065 D. The average grain diameter of the test material is approximately 1.4×10^{-3} in. The minimum stress which will form dislocation loops is

$$\tau = \frac{G\lambda\alpha}{\ell_o} \cong 10 \times 10^3 \text{ lb/in.}^2$$

Then the minimum value of P_o, corresponding to the mean value of L, is

$$P_o = \frac{\tau L}{B} \cong 35.$$

Thus, only a small error is introduced by setting $P_o - 1 = P_o$. The minimum value of the equilibrium number of dislocations, n, corresponding to this value of P_o is approximately 34. Thus, the assumption that the n dislocations may be represented by a continuous distribution between the source and grain boundary should not introduce any appreciable errors in the above calculations. Therefore, the form of equation 16 is

essentially correct, and the equilibrium microstrain observed in the test material is explainable by means of the dislocation model.

The residual microstrain observed after the test stress is removed may be qualitatively explained by the dislocation model. When the stress is removed before yielding occurs, the dislocation loops which have been formed collapse toward the source. Obstructions within the grains, such as inclusions and foreign atoms which had been previously passed by the dislocation loops with the aid of the applied stress, stop the collapse of a number of the loops, thus resulting in residual microstrain.

The recovery phenomenon and the increase in delay times for the material previously subjected to stress pulse and aging cycles may be qualitatively explained by the dislocation model. If the specimen is aged before the load is reapplied, an atmosphere of interstitial atoms will anchor the remaining loops. Thus, additional obstructions are produced which prevent yielding during the next stress pulse. When the stress is reapplied and held constant, the delay time for the initiation of yielding should be increased over the delay time for the original material.

The reduction of yield point with an increase in grain size, observed in mild steel (26), may also be qualitatively explained by this dislocation model. An increase in the grain size increases the value of L so that for a given applied stress, F_o is increased. Then, by equation 7, n is correspondingly increased. Therefore, the stress at a grain boundary due to the array of dislocations is increased. Thus, the resistance of the grain boundaries in coarse-grained material would be overcome at a lower value of the applied stress.

The approximations employed in the above analysis of the dislocation model do not permit a reliable estimate of the stress at the grain boundaries due to an array of dislocations. Therefore, the dependence of yield stress on grain size cannot be quantitatively determined by the methods developed above.

SUMMARY AND CONCLUSIONS

The results of the repeated stress-pulse tests on annealed low-carbon steel show that a definite recovery from the effects of the previous stress-pulse takes place when the combination of time and temperature between stress-pulses is sufficient. For aging periods longer than the critical recovery time at a given aging temperature, repeated stress-pulse and aging cycles do not produce yielding. For aging periods shorter than the critical recovery time, the specimen yields when the cumulative time at stress is approximately equal to the normal delay time. This recovery process is found to be associated with an activation energy corresponding to the activation energy of strain aging and diffusion of carbon and nitrogen in the steel. The repeated stress-pulse and aging treatment stabilizes the material such that the delay times are increased for the same stress.

Sensitive strain measurements under conditions of rapid loading and stress-pulses indicate that a plastic and anelastic microstrain of approximately 30×10^{-6} in./in. precedes the yield strain. The total microstrain produced by stresses less than the yield stress is a function of stress and increases with stress until a microstrain of approximately 30×10^{-6} in./in. is reached at the yield stress.

The recovery phenomenon and the increase in delay times for the previously stressed and aged material may be attributed to the diffusion of carbon and nitrogen to the dislocations which have been displaced, thus stabilizing the array of dislocations for the particular stress condition. The theory of Cottrell and Bilby adequately predicts

the experimental critical recovery times.

The experimentally observed microstrain is quantitatively explained by a dislocation-generating mechanism. An electrostatic analogy has been used to analyze the properties of the dislocation model.

It is suggested that the dislocation model be further studied to determine whether or not it can quantitatively describe the dependence of yield stress on grain size. The electrostatic analogy used in the analysis of the dislocation model is incapable of predicting this dependence.

REFERENCES

(1) J. Muir, "On the Recovery of Iron from Overstrain," Philosophical Transactions of the Royal Society of London (1900), Sec. A, Vol. 193, Part 1, p. 1.

(2) E. S. Davenport and E. C. Bain, "The Aging of Steel," Transactions, American Society for Metals, (1935), Vol. 23, p. 1047.

(3) J. R. Low, Jr. and M. Gensamer, "Aging and the Yield Point in Steel," Transactions, American Institute of Mining and Metallurgical Engineers (1944), Vol. 158, p. 207.

(4) A. N. Holden and J. H. Hollomon, "Homogeneous Yielding of Carburized and Nitrided Single Iron Crystals," American Institute of Mining and Metallurgical Engineers, Journal of Metals, (February 1949), Metals Transactions, Vol. 185, p. 179.

(5) H. Schwartzbart and J. R. Low, Jr., "The Yielding and Strain Aging of Carburized and Nitrided Single Crystals of Iron," American Institute of Mining and Metallurgical Engineers, Journal of Metals (September 1949), Metals Transactions, Vol. 185, p. 637.

(6) A. H. Cottrell, "Effect of Solute Atoms on the Behavior of Dislocations," Report of a Conference on Strength of Solids, Physical Society of London (1948).

(7) A. H. Cottrell, "The Yield Point in Single Crystal and Polycrystalline Metals," Symposium on the Plastic Deformation of Crystalline Solids, Mellon Institute (1950).

(8) F. R. N. Nabarro, "Mechanical Effects of Carbon in Iron," Report of a Conference on Strength of Solids, Physical Society of London (1948).

(9) A. H. Cottrell and B. A. Bilby, "Dislocation Theory of Yielding and Strain Aging of Iron," Proceedings, Physical Society of London (1949), Sec. A., Vol. 62, Part 1, p. 49.

(10) D. S. Wood and D. S. Clark, "The Design and Construction of a Hydro-Pneumatic Machine for Rapid Load Tensile Testing," Report No. I submitted to U. S. Air Force, Air Materiel Command, 21 May 1947.

REFERENCES (continued)

(11) D. S. Wood and D. S. Clark, "The Influence of Rapid Load and Time at Load on the Tensile Properties of Several Alloys," Report No. II submitted to U. S. Air Force, Air Materiel Command, 30 June 1948.

(12) D. S. Clark and D. S. Wood, "The Time Delay for the Initiation of Plastic Deformation at Rapidly Applied Constant Stress," Proceedings American Society for Testing Materials (1949), Vol. 49, p. 717.

(13) D. S. Wood and D. S. Clark, "The Influence of Stress and Temperature on the Time for the Initiation of Plastic Deformation in an Annealed Low-Carbon Steel," First Technical Report submitted to Office of Naval Research, Contract N6onr-24418 (June 1949), Transactions American Society for Metals (1951), Vol. 43, p. 571.

(14) D. S. Wood and D. S. Clark, "Delayed Yield in Annealed Steels of Very Low Carbon and Nitrogen Content," Second Technical Report under Office of Naval Research, Contract N6onr-24418 (August 1950), Paper Presented at the Thirty-third Annual Convention of the American Society for Metals, Detroit, October 1951.

(15) D. S. Wood and D. S. Clark, "Delayed Yielding in Annealed Mild Steel With Special Reference to Yielding at Low Temperatures," Fourth Technical Report under Office of Naval Research, Contract N6onr-24418 (December 1951).

(16) K. Stanley, "The Diffusion and Solubility of Carbon in Alpha Iron," Transactions, American Institute of Mining and Metallurgical Engineers (1949), Vol. 185, p. 752.

(17) C. Wert and C. Zener, "Interstitial Atomic Diffusion Coefficients," Physics Review (1949), Vol. 76, Ser. 2, p. 1169.

(18) L. J. Dijkstra, "Precipitation Phenomena in the Solid Solutions of Nitrogen and Carbon in Alpha Iron Below the Eutectoid Temperature," Transactions, American Institute of Mining and Metallurgical Engineers (1949), Vol. 185, p. 252.

REFERENCES (continued)

(19) B. L. Averbach, Discussion of a Paper by A. H. Cottrell, Symposium on the Plastic Deformation of Crystalline Solids, Mellon Institute (1950).

(20) A. N. Holden, "Dislocation Collision and the Yield Point of Iron," Transactions, American Institute of Mining and Metallurgical Engineers (1952), Vol. 194, p. 182.

(21) F. C. Frank and W. T. Read, "Multiplication Processes for Slow Moving Dislocations," Physics Review (1950), Vol. 79, p. 722.

(22) J. S. Koehler, "On the Dislocation Theory of Plastic Deformation," Physics Review (1941), Vol. 60, p. 397.

(23) Eshelby, Frank, and Nabarro, "Equilibrium Arrays of Dislocations," Philosophical Magazine (1951), Vol. 42, p. 351.

(24) W. R. Smythe, "Static and Dynamic Electricity," First Edition, McGraw-Hill Book Company, Chapter IV, p. 62.

(25) G. I. Taylor, "Mechanism of Plastic Deformation of Crystals," Proceedings of the Royal Society (1934), Vol. 145, p. 362.

(26) C. A. Edwards and L. B. Pfeil, "The Tensile Properties of Single Iron Crystals and the Influence of Crystal Size Upon the Tensile Properties of Iron," Journal of the Iron and Steel Institute (1925), Vol. 112, p. 79.